

Inhibition of Calcium Oxalate Monohydrate Crystallization
Using Organic Growth Modifiers

A Thesis

Presented to

the Faculty of the Department of Chemical and Biomolecular
Engineering

University of Houston

In Partial Fulfillment

of the Requirements for the Degree

Master of Science

in Chemical and Biomolecular Engineering

by

Jihae Chung

May 2013

Inhibition of Calcium Oxalate Monohydrate Crystallization Using Organic Growth
Modifiers

Jihae Chung

Approved:

Dr. Jeffrey D. Rimer, Assistant Professor,
Chemical and Biomolecular Engineering

Committee Members:

Dr. Megan Robertson, Assistant Professor,
Chemical and Biomolecular Engineering

Dr. Ognjen Miljanic, Assistant Professor,
Department of Chemistry

Dr. Suresh K. Khator, Associate Dean,
Chair of Cullen College of Engineering

Dr. Micheal P. Harold, Professor,
Chair of Chemical and Biomolecular
Engineering

Inhibition of Calcium Oxalate Monohydrate Crystallization Using
Organic Growth Modifiers

An Abstract

of a

Thesis

Presented to

the Faculty of the Department of Chemical and Biomolecular
Engineering

University of Houston

In Partial Fulfillment

of the Requirements for the Degree

Master of Science

in Chemical and Biomolecular Engineering

by

Jihae Chung

May 2013

Abstract

Inhibition of calcium oxalate monohydrate (COM), the most common component in human kidney stone diseases, was investigated using various structural derivatives of citrate, a known inhibitor of COM crystallization. Bulk crystallization studies revealed the specific binding of modifiers to COM crystal surfaces. Kinetic studies were performed to quantify both the efficacy and potency of growth inhibitors. These studies demonstrated that increased number of hydroxyl and carboxyl groups play a crucial role in interacting with specific COM crystal surface. Designing effective inhibitors require a fundamental understanding of modifier-crystal interactions at the molecular level. Consequently, we have used in situ AFM to observe the COM surface growth in the absence and in the presence of a growth inhibitor. Results obtained in this study may serve as a general platform to investigate the molecular recognition between modifiers and COM crystal surfaces as a step towards designing preventative drugs for kidney stone disease.

Table of Contents

| | |
|--|------|
| Abstract | v |
| Table of Contents | vi |
| List of Figures | viii |
| List of Tables | xii |
| 1. Introduction | 1 |
| 2. Experimental Methods | 7 |
| 2.1 Materials | 7 |
| 2.2 Calcium oxalate monohydrate crystallization | 8 |
| 2.3 Calcium-EDTA titration | 9 |
| 2.4 Ion selective electrode measurements | 11 |
| 2.5 Microscopy | 12 |
| 2.6 Atomic force microscopy | 14 |
| 3. Establishing a Standard Protocol for Assessing Organic Growth Monohydrate Efficacy | 16 |
| 3.1 Effect of HCl and NaOH addition on COM crystallization | 19 |
| 3.2 Effect of HEPES buffer on COM crystallization | 21 |
| 3.3 Calcium oxalate monohydrate solubility: Experimental | 23 |
| 3.4 Calcium oxalate monohydrate solubility: Theoretical calculations | 24 |
| 4. Molecular Analogues of Citrate | 30 |
| 4.1 Structural mapping of organic growth modifiers | 30 |
| 4.2 Effect of organic growth modifiers on COM crystallization | 33 |
| 4.3 Efficacy of organic growth modifiers | 38 |
| 4.4 Potency studies | 40 |
| 5. Design of Tailored Peptides | 47 |
| 5.1 High-throughput peptide synthesis | 49 |
| 5.2 Effect of peptides on COM crystal habit | 50 |
| 6. Interfacial Studies of Calcium Oxalate Monohydrate Crystal Growth | 55 |

| | |
|--|----|
| 6.1 Measurement of step advancement on the (010) surface | 56 |
| 6.2 Effect of chondroitin sulfate on COM crystal growth | 59 |
| 7. Conclusion | 63 |
| References | 65 |

List of Figures

| | |
|--|----|
| Figure 1-1. Schematic of a calcium oxalate monohydrate crystal. Crystals formed <i>in vivo</i> or prepared <i>in vitro</i> have three crystallographically significant faces: (100) basal surface, (010) sides, and {12-1} apical surfaces. COM crystals exhibit a hexagonal platelet morphology with a $P2_1/c$ space group. | 2 |
| Figure 2-1. Raw data of concentration of free calcium ion in solution using an ion selective electrode. (A) Temporal depletion of calcium ion. (B) Difference between the concentration at the initial point and the concentration at each time point in (A). The initial slope was used to estimate the COM growth rate. | 12 |
| Figure 2-2. SEM image of the basal surface, (100) plane, of a COM crystal with the length (L) and width (W) labeled. The aspect ratio reported in this study is equal to L/W | 13 |
| Figure 3-1. Effect of pH on COM crystallization is shown above. Bar graphs on the left (A) shows the aspect ratio ($[001]/[010]$) of crystals as a function of pH and bar graph on the right (B) shows the averaged length ($[001]$) of crystals. Error bars equal one standard deviation. | 20 |
| Figure 3-2. Effect of HEPES buffer on COM crystallization. Bar graphs in (A) are the aspect ratio ($[001]/[010]$) of crystals as a function of pH, and those in (B) are the averaged length ($[001]$) of crystals. Error bars equal one standard deviation. | 21 |
| Figure 3-3. Optical micrographs of (A) control COM crystals and (B) crystals prepared with HEPES (images were taken in transmittance mode). AFM images (C | |

and D) show representative surfaces of control crystals (C) and COM crystals in HEPES (D). 23

Figure 3-4. Solubility of COM crystals as a function of pH. Solutions were prepared with initial pH in the range of 4.3 to 10. The pH changed over the course of COM crystallization due to the acid dissociation of oxalate. Aliquots of the mother liquor were taken and analyzed by EDTA titration. Here we report the average of three titrations for day 4 (●), day 8 (▲) and day 12 (◆). Error bars equal two standard deviations. 25

Figure 3-5. Solubility COM crystals of both experimental and calculated values. (A) The concentration of free calcium ions as a function of pH for experimental (symbols) and theoretical (line). (B) The theoretical concentrations of three oxalate species. 29

Figure 4-1. Structural mapping of the OGMs used in this study, which include: 1-oxalic acid, 2-malonic acid, 3-succinic acid, 4-glutaric acid, 5-adipic acid, 6-malic acid, 7-tartaric acid, 8-tricarballic acid, 9-hydroxy methylglutaric acid, 10-citric acid, 11-hydroxycitric acid, 12-dimethyl hydroxyglutaric acid, 13-butanetetracarboxylic acid. 32

Figure 4-2. Effect of selected OGMs on COM crystallization. (A) The bar graph shows the length-to-width aspect ratio (or $[001]/[010]$) of COM crystals as a function of different OGMs. (B) The bar graph shows the average length (or $[001]$ dimension) of COM crystals. All measurements were done with ca. 70 crystals from one batch except for control which was done with five different batches. Error bars equal one standard deviation. 37

| | |
|--|----|
| Figure 4-3. Molecular topology of three crystallographically significant planes of calcium oxalate monohydrate: (100), (010) and (12-1). (A) Structures viewed normal to the plane, and (B) a side profile viewed along the plane. Note the different orientation of oxalate molecules in each plane (dashed circles). | 38 |
| Figure 4-4. Percent inhibition of selected OGMs on COM crystallization at 25°C as measured <i>in situ</i> using a calcium ion-selective electrode. Data were averaged from at least five different measurements. Error bars equal two standard deviations. | 39 |
| Figure 4-5. Aspect ratio (A) and [001] length (B) of COM crystals prepared with different concentrations of TCA, CA, and HCA. Concentrations used for this study were 0, 1, 5, 10, 20 and 60 µg/mL. Each measurement was done from ca. 70 crystals. Error bars equal one standard deviation. | 43 |
| Figure 4-6. Optical micrographs of crystals prepared with CA at 10 µg/mL (A), 20 µg/mL (B), 60 µg/mL (C), and crystals prepared with HCA at 10 µg/mL (E), 20 µg/mL (F), 60 µg/mL (G). Scanning electron micrographs of crystals with 60 µg/mL-CA (D) and 60 µg/mL-HCA (H) are shown. All scale bars indicate 30 µm. | 44 |
| Figure 4-7. Percent inhibition of crystals prepared with different concentrations of TCA, CA, and HCA. The following concentrations of OGM were examined: 0, 1, 5, 10, 20, and 60 µg/mL. Error bars equal two standard deviations and lines are interpolations of the data. | 46 |
| Figure 5-1. Optical micrographs of crystals prepared with different peptides. (A) D1; (B) D2; (C) D3; (D) D4; (E) D5; (F) D6; (G) D7; (H) D8; (I) D9; (J) D10. All images were taken under reflectance mode. | 53 |

| | |
|---|----|
| Figure 5-2. Effect of peptides on the aspect ratio (A), length (B), and the population (C) of COM crystals. Each measurement was performed with three separate batches. Error bar equals one standard deviation. | 54 |
| Figure 6-1. Demonstration of an AFM single-line scan method. The step velocity was obtained by measuring the distance between each step of the hillock and a reference line (labeled in B). The images shown here are in deflection mode. | 58 |
| Figure 6-2. Consecutive deflection mode AFM images of growth hillocks growing in supersaturated calcium oxalate solution. The step velocity was obtained by measuring the change in step position with images taken in succession. | 59 |
| Figure 6-3. <i>In situ</i> AFM images of growth hillocks on a (010) surface. Time-elapsed images were taken at an initial time (A) and after 10 minutes of growth (B). Images C – E show the effect of 1 $\mu\text{g/mL}$ -C ₄ S on hillock growth. These studies reveal the formation of 2-D islands (C) and an increase in the height of steps (D), as indicated by the arrows. Images F and G show the effect of 5 $\mu\text{g/mL}$ C ₄ S on hillock growth. After one minute growth is complete arrested (G). Image H shows the recovery of growth hillocks upon removal of C ₄ S from the growth solution. Scale bars indicate 1 μm | 62 |

List of Tables

| | |
|--|----|
| Table 2-1. List of chemicals used to examine COM crystallization. | 7 |
| Table 3-1. Reported pKa values of OGMs at 25°C. | 17 |
| Table 3-2. Structures of buffering compounds. | 19 |
| Table 4-1. List of OGM structures and their effect on the aspect ratio and the length of COM crystals. | 35 |
| Table 5-1. List of peptide sequences used in this study. | 50 |
| Table 6-1. Reported values of COM step velocity on the (010) surface. | 59 |

1. Introduction

Nephrolithiasis is a common renal pathological disorder that influences about 15% of the U.S. population. Unfortunately, while the number of inflicted people is on the rise, there has been no significant development in treatments for the past 30 years [1]. About 80% of all nephrolithiasis cases involve calcium salts in the form of calcium oxalate or calcium phosphate. Calcium oxalate is the most predominant compound of kidney stones, and can be found in three hydrate forms: calcium oxalate monohydrate (COM), dihydrate (COD) and trihydrate (COT). COM is the most thermodynamically stable hydrate and the most common component in kidney stones. COD is less thermodynamically stable, but is observed in urine and is proposed to be a benign crystalline form of calcium oxalate (as evidenced by its low content in human kidney stones) [2, 3]. Crystals of COT are rare and less physiologically relevant [4].

Formation of renal stones is a complex process involving multiple steps and various components. There are four processes associated with the formation of COM stones: crystal nucleation, growth, aggregation, and attachment (i.e., retention) of crystals and/or aggregates to epithelial cells [4]. There are many factors that can lead to an increased incidence rate of COM stones [5]: hypercalciuria [6, 7], hyperoxaluria [8, 9] and dehydration [10, 11]. Hypercalciuria is the most common metabolic abnormality found in patients of nephrolithiasis, which raises the supersaturation of calcium oxalate in urine that can ultimately promote nucleation and growth of crystals. Likewise, hyperoxaluria is a condition affecting ca. 30% of kidney stone patients and can increase the risk of stone formation. In most patients the hyperoxaluria is of mild

to moderate level and it is usually the result of dietary overindulgence of oxalate [12]. Also, high fluid intake dilutes urine, which reduces the propensity for the crystallization of calcium salts in urine by lowering the urinary saturation of calcium and oxalate. Calcium oxalate monohydrate crystals have a $P2_1/c$ space group ($a = 6.290 \text{ \AA}$, $b = 14.5803 \text{ \AA}$, $c = 10.116 \text{ \AA}$) [13] and exhibit a thin hexagonal platelet morphology with three crystallographically relevant surfaces: (100), (010) and $\{12-1\}$.

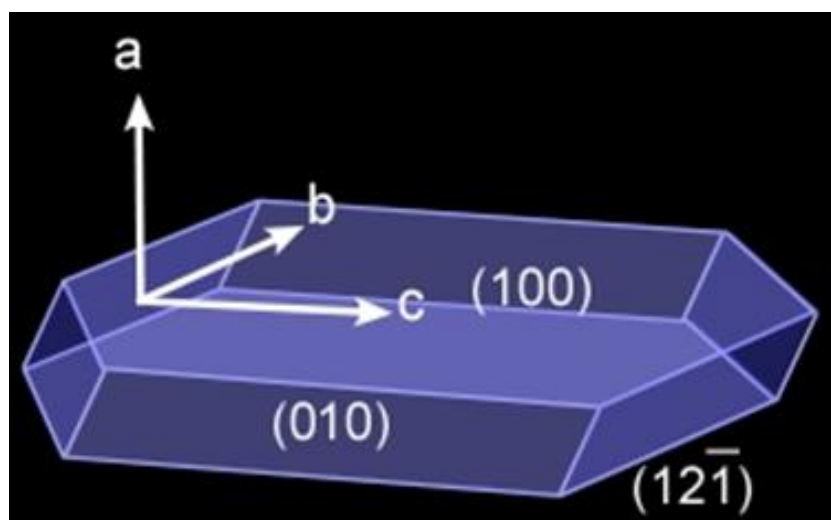


Figure 1-2. Schematic of a calcium oxalate monohydrate crystal. Crystals formed *in vivo* or prepared *in vitro* have three crystallographically significant faces: (100) basal surface, (010) sides, and $\{12-1\}$ apical surfaces. COM crystals exhibit a hexagonal platelet morphology with a $P2_1/c$ space group.

Researchers have found that some components in human urine have inhibitory effects on calcium oxalate nucleation, growth, and aggregation. Early studies by Asplin and coworkers showed that the urinary protein nephrocalcin (NC) reduced crystal aggregation by comparing the crystals formed in the urine of stone-forming patients and that of a control group. The amino acid sequence of NC contains acidic glycoprotein residues that contain α -carboxyglutamic acid moieties [14]. Asplin's studies revealed that crystals from stone-forming patients were agglomerates whereas

those from the control group were in the form of single crystals. NC extracted from the organic matrix of human stones from nephrolithiasis patients abnormally lacked Glu residues [15], which could affect the ability of NC to bind to the surface of COM crystals via calcium bridges between the carboxylic acid groups of the protein and oxalate groups on the COM surface: $\text{COOH (Glu)} \dots \text{Ca}^{2+} \dots \text{HOOC (oxalate, COM)}$ [16].

It has been proposed that the moieties of crystal growth inhibitors can be divided into two general types: a binder and a perturber [17-19]. A binder will interact with the crystal surface and bind to the crystal surface, whereas the perturber will sterically hinder the solute molecules from attaching to the crystal surface [20]. There have been a number of proposed calcium oxalate inhibitors in the literature, including (but not limited to) citrate [21, 22], amino acids [23], peptides [24], peptoids, and common urinary constituents [25]. Many groups have studied the role of urinary proteins and glycosaminoglycans as putative inhibitors of COM crystallization [26] and aggregation [27-29]. Among the most commonly studied constituents are osteopontin (OPN) [30-33], Tamm-Horsfall protein (THP) [34], transferrin [35], serum albumin [36, 37], and chondroitin [38]. High efficacy growth inhibitors of COM all share a common trait – a high percentage of negatively-charged functional groups (i.e., phosphates or carboxylic acids present in glutamic acid, aspartic acid, and sugar residues).

As previously mentioned, negatively-charged moieties of growth inhibitors interact strongly with the negatively-charged COM surfaces through the formation of calcium bridges between the inhibitor and crystal. For example, the small organic molecule citrate (which contains three carboxylic acid groups) is an over-the-counter

supplement commonly administered to stone patients. Citrate has been extensively studied due to its moderate inhibitory effect of COM crystallization. It was found that citrate was capable of forming a complex with calcium and also binds the crystal surface [16]. Ryall and coworkers investigated the adsorption affinity of amino acids on calcium oxalate crystal [39]. They prepared a saturated aqueous solution of calcium oxalate and placed COM crystals and single amino acid in the solution. After the crystals were in contact with amino acids for 15 hours, the supernatant solutions were filtrated and the remaining concentration of amino acid was monitored using HPLC. From these studies it was shown that the most effective amino acids were aspartic acid, glutamic acid, and γ -carboxyglutamic acid (i.e., these amino acids most strongly adsorbed to COM crystal surfaces). Based on the strong adsorption affinity of dicarboxylic acids and tricarboxylic acids, it was proposed that the proteins rich in such amino acids would have higher impact on crystals compared to than those with fewer negatively-charged groups [39].

This observation is consistent with clinical and *in vivo* studies revealing highly anionic proteins, such as OPN, are effective inhibitors of stone formation [40, 41]. OPN is a ubiquitous protein in physiological processes (e.g., bone formation) and is a potent inhibitor of COM crystallization owed to its high percentage of aspartic acid groups as well as phosphates [42, 43]. It is found that OPN is capable of inhibiting all four critical steps of COM formation: nucleation, growth, aggregation, and retention. There have been many studies to elucidate the effect of spatial Glu and Asp patterning in the primary amino acid sequence of OPN through techniques that include posttranslational modification to remove phosphate groups from peptide segments of the protein. For instance, phosphorylation of OPN was shown to greatly enhance the

inhibition of crystal growth. The influence of protein modification has also been noted for THP, the most abundant protein in urine and a major component of the stone matrix. The reported effects of THP on COM crystallization and aggregation are widely varying in their claims of THP acting as a stone inhibitor [41, 44-46] and promoter [47, 48], due in part to the large variation in sialic acid content (i.e., the functional groups present in glycosyl side groups of THP) [49]. Several clinical studies have shown that when comparing THP extracted from stones of former stone-forming patients and a control group, the level of sialic acid in THP was reduced for stone-forming patients [50, 51]. Viswanathan et al. investigated the relative effects of THP and desialylated THP (or ds-THP) on crystal aggregation and reported that the latter promoted COM aggregation [49]. They hypothesized that sialic acid (consisting of one carboxyl group) contributed to the overall negative charge of THP, and that by eliminating these residues from the protein, the modified protein may function as a promoter of COM aggregation.

To this end, we have judiciously selected a series of organic growth modifiers and a tailor designed peptide library to examine their effects on COM crystallization and compare the effects of each modifiers in the following chapters. Chapter 2 will discuss the experimental methods and conditions used in this study in investigating the effects of modifiers and similarly in Chapter 3, preliminary studies in establishing a standard protocol which was required to properly observe the effects of modifiers will be discussed. Chapter 4 contains studies of effects of citrate and structural derivatives of citrate (which will be called organic growth modifiers, OGMs) on COM crystallization i.e., the specificity of modifiers and their effect on kinetics of COM crystals. Chapter 5 explores the effect of tailor designed 18-mer peptides in

crystal habit and also compares the effects of different sequence while Chapter 6 presents preliminary studies on COM crystal growth rate and the interfacial interaction between a growth modifier and COM crystal surface. Finally Chapter 7 will summarize the work and give conclusions.

2. Experimental Methods

2.1 Materials

All materials used in this study were purchased from several different chemical manufacturers and were used as purchased without further purification. Table 2-1 shows the list of chemicals used for all studies reported herein. All aqueous solutions were prepared with deionized water (Aqua Solutions, RODI-C-12A purification system, 18.2 M Ω).

Table 2-1 List of chemicals used to examine COM crystallization.

| Name | Manufacture | Purity |
|----------------------------|--------------------|---------------|
| Calcium chloride dihydrate | Sigma Aldrich | 99% |
| Sodium oxalate | Sigma Aldrich | 99% |
| Sodium chloride | J.T. Baker | 99.5% |
| Oxalic acid | Sigma Aldrich | 99% |
| Malonic acid | Sigma Aldrich | 99% |
| Succinic acid | Sigma Aldrich | 99% |
| Glutaric acid | Aldrich | 99% |
| Adipic acid | Sigma | 99% |
| Tricarballic acid | Aldrich | 99% |

Table 2-1 List of chemicals used to examine COM crystallization (continued).

| Name | Manufacture | Purity |
|---|--------------------|---------------|
| Potassium hydroxycitrate tribasic monohydrate | Sigma | 95% |
| 1,2,3,4-Butanetetracarboxylic acid | Aldrich | 99% |
| 3-Hydroxy-3-methylglutaric acid | Aldrich | 98% |
| DL-malic acid | Aldrich | 99% |
| Potassium tartarate dibasic hemihydrate | Sigma Aldrich | 99% |
| Dimethyl 3-hydroxyglutarate | Aldrich | 98% |
| Sodium citrate dihydrate | Sigma Aldrich | 99% |
| Sodium hydroxide | Sigma Aldrich | 98% |
| Hydrochloric acid | Sigma Aldrich | 37% |
| HEPES sodium salt | J.T. Baker | 99.6% |

2.2 Calcium oxalate monohydrate crystallization

Supersaturated calcium oxalate monohydrate solution was prepared by mixing an equal volume of two previously prepared aqueous 10 mM stock solutions of calcium chloride and sodium oxalate. A 150 mM concentration of sodium chloride was used to increase the ionic strength of the solution. After sodium chloride was fully dissolved in water, calcium chloride was added while the solution was stirred at the rate of 400 rpm. The solution was placed in oven set at 60°C for one hour prior to

the dropwise addition of sodium oxalate (while stirring). COM crystallization was performed using a total calcium oxalate concentration of 0.7 mM (i.e., supersaturation = 5.4, solubility product = 1.66×10^{-9} (25°C) [24, 52]). Crystals were prepared at 60°C rather than at room temperature or physiological body temperature (ca 37°C) to expedite the growth of large crystals on a reasonable timescale (i.e., 24 to 72 hours). Following the addition of sodium oxalate a clean glass slide was placed at the bottom of glass vial to collect the resulting crystals. The final volume of the growth solution for each batch was 10 mL.

The procedure for preparing COM crystals in the presence of any additive (i.e., organic growth modifiers, HEPES buffer, hydrochloric acid, or sodium hydroxide) was similar to the procedure for control crystals. Stock solutions for each additive were prepared in advance and the amount of water was calculated in order to achieve a final volume of 10 mL for each batch. The same procedure was applied for pH correction studies. Hydrochloric acid or sodium hydroxide stock solutions were prepared and were added to establish a desired pH of COM growth solutions. The pH of each COM growth solution (with or without additives) was confirmed using a pH meter (ThermoScientific, ORION 3 STAR pH Benchtop with Orion 8102BNUWP probe).

2.3 Calcium-EDTA titration

Calcium-EDTA titration was performed to quantify the solubility of COM crystals with different solution pH. It is a simple procedure that is most commonly used to measure the hardness of water and gives reasonable resolution of calcium ion concentration (i.e., ppm range), which is. Ethylenediaminetetraacetic acid (EDTA) is

a chelating agent and weak acid with four carboxylic acid residues that easily dissociate at physiological pH. EDTA complexes metal ions in 1:1 mole ratio. Eriochrome Black T is one of the commonly used indicators for EDTA titration since it forms a wine-red complex with magnesium ion (MgIn^-) in alkaline solution. During titration, EDTA chelates calcium ions in the solution and the indicator remains wine-red MgIn^- until the end of titration when the entire number of free calcium ions is zero (i.e., fully chelated by the EDTA molecules) and excessive EDTA chelates the magnesium (MgIn^-), which results in a color change (the indicator reverts back to its acid form, which is sky blue).

Calcium-EDTA titration was performed with nine solutions of the same composition, but with different pH in the range $4 < \text{pH} < 10$ (where the pH was adjusted using either HCl or NaOH). Solutions were placed in a water bath at 30°C for a two week period. Aliquots of the solution were extracted every 4 days. The solutions were filtered with $0.45\ \mu\text{m}$ nylon membrane (Life Sciences, Acrodisc® Premium 25 mm Syringe Filter) prior to analysis. A standard solution of EDTA (0.1 M) was prepared and diluted with deionized water. Eriochrome Black T was used as an indicator to observe the completion of EDTA titration. NaOH was added to each titration sample to ensure full dissociation of EDTA carboxylic acid groups prior to analysis. The samples were vigorously stirred during titration to ensure distinct color change was observed. A minimum of three measurements were performed for each batch.

2.4 Ion selective electrode measurements

A calcium ion selective electrode (ISE, ThermoScientific with Orion 9720BNWP ionplus® electrode) was used to measure the effect of organic growth modifiers on the kinetics of COM crystallization. ISE measures the concentration of free calcium ions in solution, which is shown in Figure 2-1A. OGM efficacy was measured by calculating the temporal depletion of calcium ion concentration (ppm range). The data was normalized by subtracting the concentration of the initial time point (see Figure 2-1B). The rate of depletion was measured by measuring the initial slope of the crystal growth curve. ISE data shown in Figure 2-1 is nonlinear, which is anticipated since the removal of calcium from solution is attributed to COM nucleation and growth, which is a nonlinear function of calcium supersaturation. To minimize the induction time for nucleation, solutions were stirred at the rate of 1200 rpm while measuring the concentration of calcium ion [53]. The efficacy of OGMs was assessed using the percent inhibition, which was calculated by comparing the reduced slopes for each OGM relative to that of the control (i.e., absence of OGM). Prior to ISE measurements, the electrode was calibrated using a standard calcium solution (0.1 M, Orion Ion Plus), which was diluted with deionized water to three concentrations: 10^{-4} , 10^{-3} and 10^{-2} M. The ionic strength of each solution was adjusted using a standard solution (ISA, Thermo Scientific), which was added in a 1:50 volume ratio of ISA-to-standard.

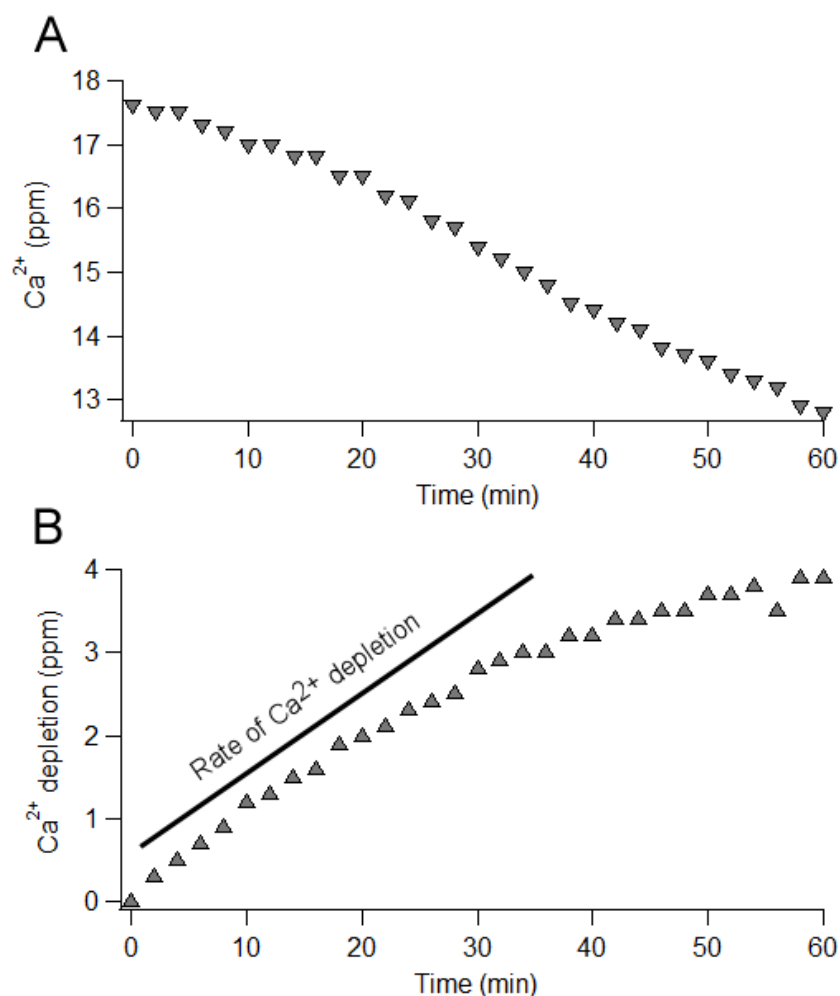


Figure 2-1. Raw data of concentration of free calcium ion in solution using an ion selective electrode. (A) Temporal depletion of calcium ion. (B) Difference between the concentration at the initial point and the concentration at each time point in (A). The initial slope was used to estimate the COM growth rate.

2.5 Microscopy

Optical microscopy was employed to observe the overall morphology of crystals retrieved from bulk crystallization and also to compare the effect of each additive on crystallization. Images were obtained using a Leica DM2500-M microscope equipped with three brightfield/darkfield objectives (10x, 20x, and 50x). The images were captured in brightfield using transmission mode, and the Leica built-in software was used to both acquire the images of crystals and measure the length

(L), width (W), and aspect ratio of crystals. In this study, the crystal length is defined as the distance between apical tips of the hexagonal basal surface (i.e., [001] length), the width of crystal is defined as the dimension along the [010] direction, and the aspect ratio is reported as the ratio of [001] to [010] lengths (or L/W , see Figure 2-2). The glass slides placed at the bottom of the COM crystallization vial collected the crystals. These slides were removed from the mother liquor, gently washed with DI water, and allowed to air dry prior to analysis. Scanning electron microscopy (SEM) was performed using a FEI 235 Dual-Beam Focused Ion-beam instrument. Electron micrographs were used to observe the size, shape, and contours of COM crystals with higher resolution. Each sample was prepared by gently pressing the glass slide containing COM crystals to an SEM sample holder with carbon tape. The sample was coated with ca. 25 nm carbon prior to analysis to reduce the effects of charging. Selected crystals with interesting features were measured using 12.0 eV and a distance of 6.902 mm.

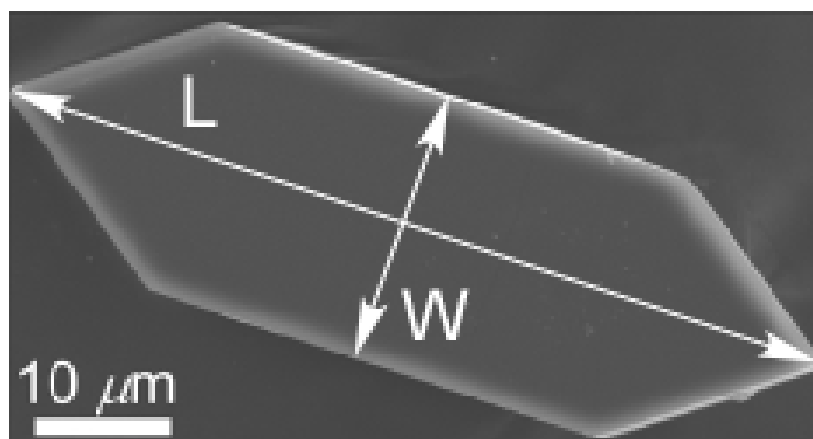


Figure 2-2. SEM image of the basal surface, (100) plane, of a COM crystal with the length (L) and width (W) labeled. The aspect ratio reported in this study is equal to L/W .

2.6 Atomic force microscopy

Atomic force microscopy (AFM, Bruker Multimode 3) was used to study the COM crystal surface topography at a nanometer length scale. Samples were mounted on a specimen disk covered with a thin layer of thermally curable epoxy (MasterBond EP21AOLV). The epoxy was partially cured using a previously reported protocol whereby the sample disk was heated in an oven for ca. 20 min at 60°C [54]. Crystals retrieved on the glass slide from bulk crystallization (section 2.2) were transferred to the precured epoxy by lightly pressing the crystals against the epoxy. The crystals were immobilized on the epoxy with the [100] direction oriented normal to the specimen surface by placing the sample in an oven at 60°C for two to three hours to completely cure the epoxy. The cantilevers used in this study were silicon nitride probes with gold reflex coating and a spring constant of 0.15 N/m (Olympus, TR800PSA).

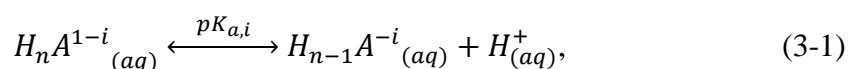
AFM was also employed to observe the kinetics of crystal growth in supersaturated calcium oxalate solutions by monitoring *in situ* the velocity of step advancement on the (010) surface of COM crystals. The experiment was designed to assess the effects of inhibitors on step growth using a fluid cell (Bruker, MTFML) to produce an environment that mimics *in situ* crystallization. The sample cell contained two ports for inlet and outlet flow to maintain constant supersaturation during AFM measurements. A silicon O-ring was used to ensure no liquid leakage would occur while solutions were being continuously replenished. A dual syringe pump (CHEMYX, Fusion 200) was used to provide in flow mixing of calcium and oxalate. To this end, two different stock solutions of calcium chloride and sodium oxalate

were prepared with concentrations of 6.0 to 8.0 mM and 0.3 to 0.4 mM, respectively. The two solutions were mixed in flow prior to entering the sample cell to minimize homogeneous nucleation and growth of COM crystals. The combination of stock solutions yielded growth solutions with composition 0.15 to 0.2 mM (or supersaturations ranging from 3.2 to 4.1). Several calcium oxalate concentrations were used to identify an ideal supersaturation for *in situ* AFM studies. The flow rate used for these studies was 0.2 mL/min. Several groups have studied COM growth using *in situ* AFM, including DeYoreo, Ward and Rashkovich, and employed different flow rates according to their purpose of work. For instance, DeYoreo's group used 2 mL/min to ensure that growth was limited by surface kinetics and not by diffusion. They noted that at a given supersaturation, the rate of step advancement did not change when the flow rate was further increased [14, 52], Ward and coworkers did not use in line flow, but replenished solutions at 5 minute intervals to maintain a relatively constant supersaturation [55]. Rashkovich's group used a constant flow rate of 0.3 – 0.5 mL/min since they reported that the rate of crystal growth and dissolution were independent of solution flow rate in this range [56, 57].

The flow rate used in this study was 0.2 mL/min, which is an order of magnitude smaller than that used by DeYoreo and similar to the value used by Rashkovich. This rate was selected at a maximum value that also minimized the effects of fluid flow on the cantilever imaging of COM crystal surfaces. It is possible that due to the lower flow rate, the rate of COM crystal growth observed in this study was influenced by mass transfer limitations; however, higher flow rates sacrificed the resolution of *in situ* images.

3. Establishing a Standard Protocol for Assessing Organic Growth Modifiers Efficacy

The organic growth modifiers (OGMs) that were used in this study are acids with multiple dissociation constants. Table 3-1 lists the molecules assessed as potential OGMs, which have carboxylic acids that dissociate at physiological conditions. The pKa is given by the following relationship,



where n is the number of carboxylate groups ($n = 0$ to 3) and i is the number of dissociated groups (or negative charge of the OGM). The molecules in Table 3-1 are structural derivatives of hydroxycitrate and citrate, which is a known growth inhibitor of COM stone formation [9, 58]. For this study, commercially available molecules were selected with varying carbon backbone length and varying number and spatial location of hydroxyl and carboxylic acid groups between the two terminal acid sites (see Figure 4-1 in Chapter 4). Notably, we wished to examine segments of hydroxycitrate and citrate to ascertain the physicochemical factors regulating OGM efficacy and their ability to interact with COM crystal surfaces.

The addition of acidic OGMs in COM growth solutions renders the pH well below physiological conditions (i.e., average urine pH = 5 - 8). The pH of solution affects the total charge of OGMs, which is a mitigating factor of OGM efficacy in COM growth inhibition studies. Moreover, lower pH leads to higher concentration of protonated oxalate ions (i.e., free molecules in solution as well as surface oxalate on COM crystals), which influences the ability of free oxalate molecules to complex with

Table 3-1. Reported pKa values of OGMs at 25 °C [15, 59].

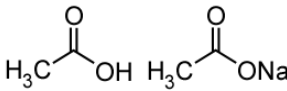
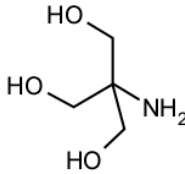
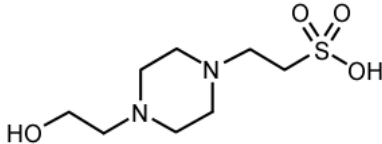
| Organic Growth Modifier | pKa₁ | pKa₂ | pKa₃ |
|--------------------------------|------------------------|------------------------|------------------------|
| Oxalic acid | 1.23 | 4.19 | |
| Malonic acid | 2.83 | 5.69 | |
| Succinic acid | 4.16 | 5.61 | |
| Glutaric acid | 4.31 | 5.41 | |
| Adipic acid | 4.43 | 5.41 | |
| Butanetetracarboxylic acid | ----- | ----- | |
| Tricarballic acid | ----- | ----- | |
| Hydroxy methylglutaric acid | ----- | ----- | |
| Citric acid | 3.09 | 4.75 | 5.41 |
| Hydroxycitric acid | ----- | ----- | |
| Dimethyl hydroxyglutaric acid | ----- | ----- | |
| DL-tartaric acid | 3.03 | ----- | |
| Malic acid | 3.4 | 5.11 | |

Note: ----- signifies data that is not reported in the literature

calcium ions at the crystal interface and can also reduce the negative charge of COM crystal surfaces. To properly study the effect of each OGM it was necessary to correct for changes in pH with OGM addition in order to match the nominal condition used for control experiments (i.e., pH 6.2). The two most common methods to adjust pH are the addition of either acid or base, such as hydrochloric acid (HCl) and/or sodium hydroxide (NaOH), or the use of a buffer. The latter is used in various applications, especially in biomedical fields. In this study, both methods of pH adjustment were

examined to select an optimum approach. There are three different buffers used in COM crystallization: Acetate buffer [56, 60, 61], tris(hydroxymethyl)aminomethane (Tris) buffer [43, 62], and hydroxyethyl piperazineethanesulfonic acid (HEPES) [38, 49, 55]. The carboxyl group in acetate buffer may interact with COM crystals via a calcium bridge, and Tris buffer has three hydroxyl groups which may interact with crystals via hydrogen bonding. Also, buffers have different pH ranges: acetate buffer (3.8 - 5.8), Tris buffer (7.5 – 9.0), and HEPES buffer (6.8 – 8.2). The buffer selected for this study was HEPES due to acidic nature of OGMs and also the pH range of HEPES buffer is within the pH range of normal urine. In order to observe the effects of pH adjustment on COM crystallization through acid (HCl) or base (NaOH) addition or via the use of HEPES buffer, bulk crystallization studies were performed to compare the morphology of COM crystals. In addition, a calcium ion selective electrode (ISE) was used to monitor the depletion of free calcium ions in solution over the course of COM crystallization in the presence of OGMs.

Table 3-2. Structures of buffering compounds.

| Name | Structure |
|----------------|--|
| Acetate buffer |  |
| Tris buffer |  |
| HEPES |  |

3.1 Effect of HCl and NaOH addition on COM crystallization

The effects of pH were first investigated by examining COM crystals prepared by the addition of either HCl or NaOH to a control solution with composition 0.7 mM CaCl_2 : 0.7 mM $\text{Na}_2\text{C}_2\text{O}_4$: 150 mM NaCl. The amounts of acid and base were selected to examine pH values between 4 and 10. The crystals were isolated on glass slides after 3 days of crystallization at 60°C. Optical microscopy was used to measure the [001] length and [010] width of the basal surfaces. This procedure was repeated a total of three times at each pH to provide adequate statistics. The average length-to-width (i.e., [001]/[010]) aspect ratios are shown in Figure 3-1A, and the average lengths are provided in Figure 3-1B. These studies revealed that pH has a marginal effect on the COM crystal aspect ratio; however, there is a noticeable, albeit small, increasing trend in aspect ratio with increasing pH. For instance, at pH 4.3 there was a 15% decrease in the aspect ratio relative to the control (pH 6.2), and at pH 10 there

was an 8% increase in the aspect ratio relative to the control. These studies also revealed that the effect of pH on the [001] length of COM crystals was more dramatic. As shown in Figure 3-1B, the crystal size increases as pH increases, such that at pH 4.3 there is a 41% decrease in length relative to the control ($40.8 \pm 8.9 \mu\text{m}$), and at pH 9 there is a 20% increase relative to the control.

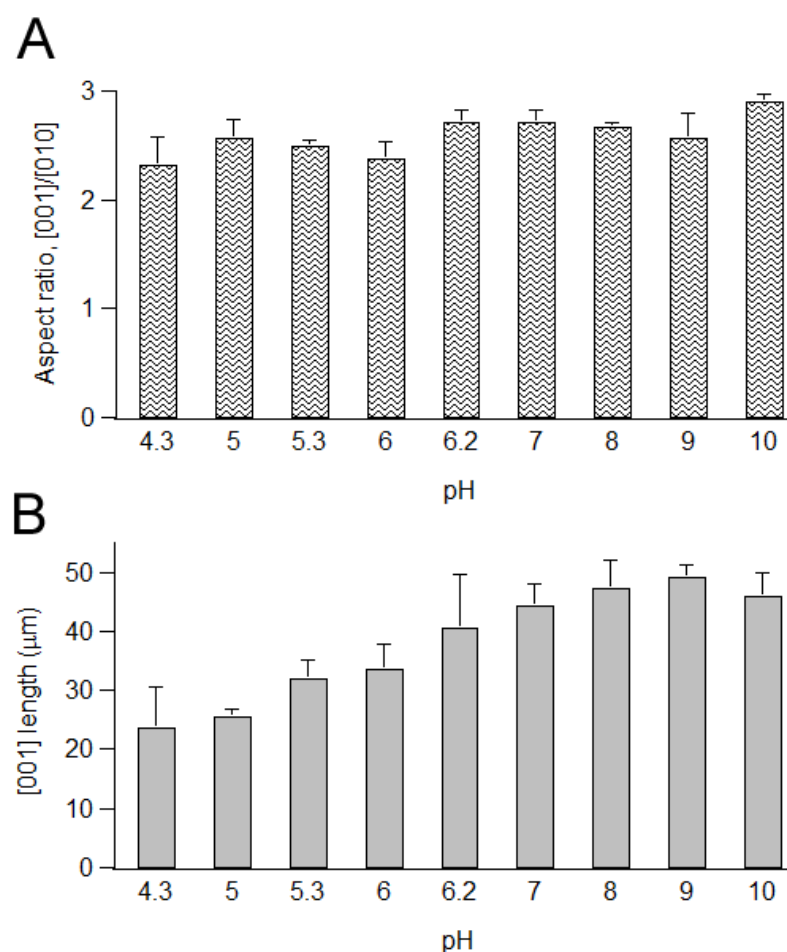


Figure 3-1. Effect of pH on COM crystallization is shown above. Bar graphs on the left (A) shows the aspect ratio ([001]/[010]) of crystals as a function of pH and bar graph on the right (B) shows the averaged length ([001]) of crystals. Error bars equal one standard deviation.

3.2 Effect of HEPES buffer on COM crystallization

The effect of HEPES buffer on the COM crystal aspect ratio and [001] length are shown in Figures 3-2A and 3-2B, respectively. The adjustable pH range through HEPES addition was restricted to pH values between 6 and 8. As shown in Figure 3-2A, the HEPES buffer did not impose strong effects on the aspect ratio of COM crystals. Notably, there is a ca. 3% decrease in aspect ratio for pH values above the control. The aspect ratios obtained by HEPES addition are similar to those obtained by the addition of NaOH at the same pH values. Similar to the previous method, HEPES buffer did alter the length of COM crystals. As shown in Figure 3-2B, there is a maximum 34% increase in [001] length.

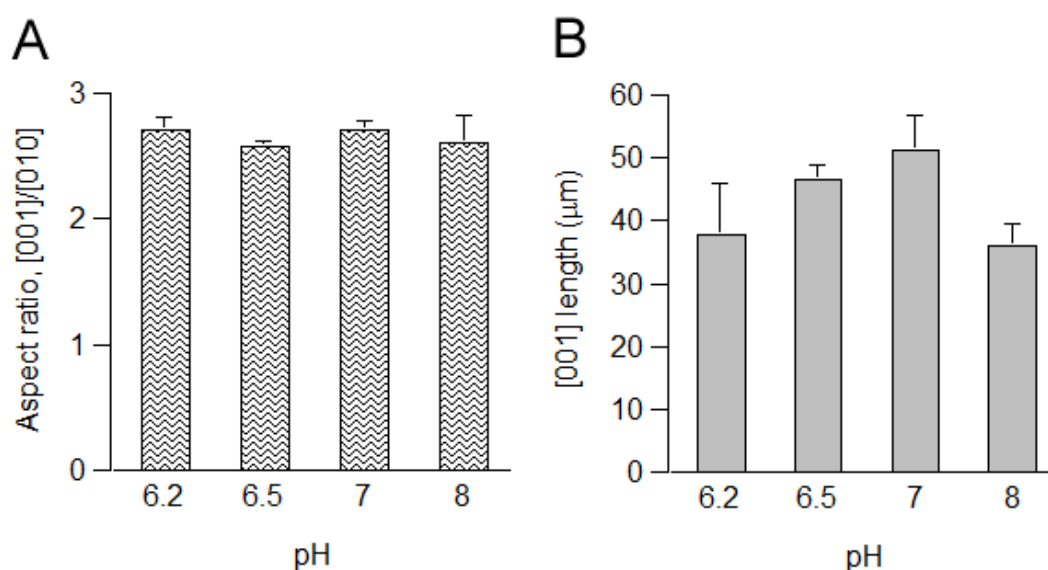


Figure 3-2. Effect of HEPES buffer on COM crystallization. Bar graphs in (A) are the aspect ratio ([001]/[010]) of crystals as a function of pH, and those in (B) are the averaged length ([001]) of crystals. Error bars equal one standard deviation.

Moreover, the basal surface of COM crystals prepared in HEPES buffer appeared to be roughened in optical micrographs compared to the smooth surfaces

obtained in control samples. Figure 3-3A and 3-3B shows the basal surfaces of COM crystals of control and COM crystals in HEPES, respectively. According to optical micrographs, the presence of HEPES in crystallization process produces more residues as opposed to the process without the HEPES buffer. Figure 3-3C and 3-3D shows the 10 μm x 10 μm AFM topographical images of control crystals and COM crystals in HEPES, respectively. The roughened surface features in the presence of HEPES buffer were observed in AFM images. Steps on the (100) basal surface, as shown in Figure 3-3D, were consistent among crystal samples. The average step height was 21.5 nm and step ledges were aligned along b-axis. The root mean square (RMS) roughness of the basal surface was 1.4 and 6.5 nm for COM crystals in the absence (control) and presence of HEPES buffer, respectively. The approximate 5-fold increase in surface roughness suggests HEPES interacts with the COM interface. HEPES buffer has one hydroxyl group (i.e., H-binding moiety) and one sulfonic acid (i.e., negatively-charged moiety), which can possibly interact with oxalate or calcium on the COM crystal surface, respectively. It is feasible that HEPES interactions with COM surfaces could interfere with OGM binding. Conversely, the adjustment of pH via the introduction of HCl or NaOH did not result in significant changes in either crystal habit or surface topography. In this regard, acid/base addition was selected as the preferred method for pH adjustment.

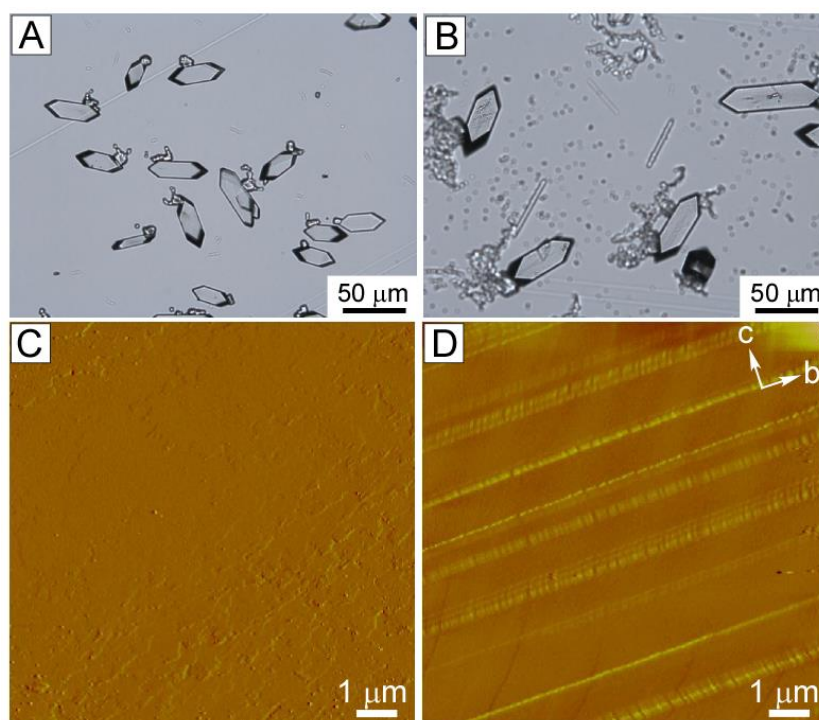


Figure 3-3. Optical micrographs of (A) control COM crystals and (B) crystals prepared with HEPES (images were taken in transmittance mode). AFM images (C and D) show representative surfaces of control crystals (C) and COM crystals in HEPES (D).

3.3 Calcium oxalate monohydrate solubility: Experimental

There have been several prior studies that explored the solubility of COM crystals as a function of pH; however, there are discrepancies in the results of those investigations. For instance, some studies report an increased solubility of COM with increasing pH [63, 64], while others report decreased solubility of COM with increasing pH [65-68]. Moreover, the conditions used in past experiments varied from pure aqueous solution to urine-like environments. For example, Streit et al. used three different urine-like solutions including Standard Reference Artificial Urine (SRAU) [69]. These solutions consisted of different compositions and concentrations of NaCl, Na₃Citrate, Na₂SO₄, MgSO₄, creatine, urea, and other constituents.

Solubility is an important determinant in the growth rate of crystals. In this regard, it was imperative that the effect of pH on COM crystal solubility be elucidated to accurately control calcium oxalate supersaturation in AFM studies (as will be discussed in Chapter 5). A simple, but reasonably accurate, titration was performed using the chelating agent ethylenediaminetetraacetic acid (EDTA) to determine the temporal changes in free calcium ion concentration in the supernatant solution of a COM growth solution at different solution pH. The acidity and basicity of a control solution was varied using either HCl or NaOH, respectively. Solutions were placed in a water bath at 30°C for a two week period. Aliquots of the solution were extracted every 4 days. The solutions were filtered with 0.45 μ m nylon membrane (Life Sciences, Acrodisc® Premium 25 mm Syringe Filter) prior to analysis. A 0.1 M EDTA standard solution was prepared and diluted with deionized water.

The measured calcium ion concentration in solutions in the range $4 < \text{pH} < 10$ is shown in Figure 3-4. According to the results of Ca-EDTA titration, the solubility of COM crystals seemed to decrease with increasing pH. On day 4 (indicated by closed circles), there were no significant pH changes in solutions. The solubility of COM crystals seemed to have a decreasing trend with increasing pH in the range $4 < \text{pH} < 6$; however, in the range $6 < \text{pH} < 10$ the solubility increased and leveled out. Fluctuations of data points within the plot on day 4 suggested that perhaps four days were not sufficiently long enough for solutions to reach equilibrium. On day 8 (indicated by closed triangles), the solubility of COM crystals seemed to decrease with increasing pH; however, the solution pH changed in the range $6 < \text{pH} < 8$ with points converging to ca. pH 7 (i.e., solutions with original pH 6 increased to pH 7 and solutions with original pH 8 decreased to pH 7). On day 12 (indicated by closed

diamonds), similar behavior was observed. The solubility of COM crystals seemed to decrease with increasing pH and a more dramatic pH change of each sample was observed. The change in solution pH may be due to dissolving of carbon dioxide in the solution in the 12 day period and also while extracting solutions every 4 days; however, it is not definitive as to why the pH of solutions changed over time.

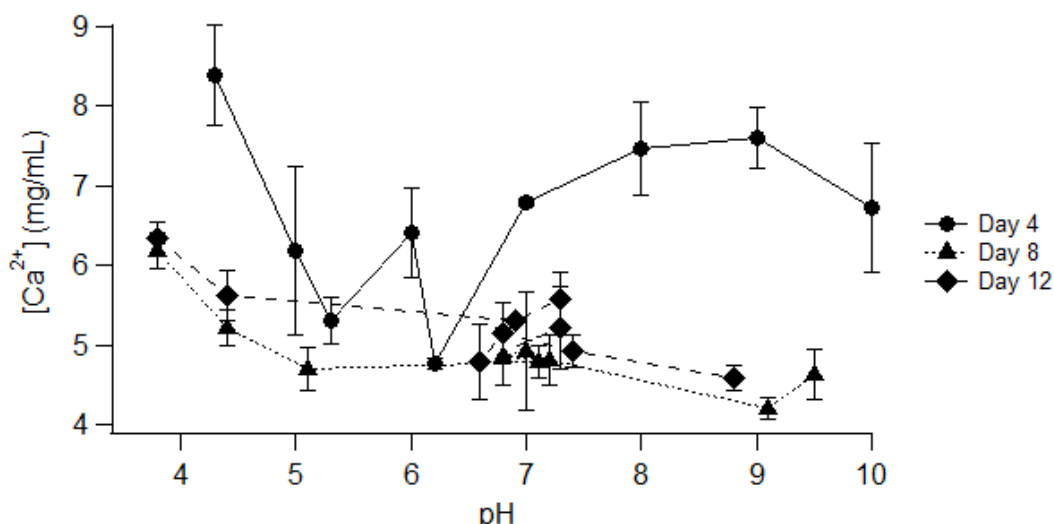


Figure 3-4. Solubility of COM crystals as a function of pH. Solutions were prepared with initial pH in the range of 4.3 to 10. The pH changed over the course of COM crystallization due to the acid dissociation of oxalate. Aliquots of the mother liquor were taken and analyzed by EDTA titration. Here we report the average of three titrations for day 4 (●), day 8 (▲) and day 12 (◆). Error bars equal two standard deviations.

3.4 Calcium oxalate monohydrate solubility: Theoretical calculations

The theoretical solubility of COM crystals was calculated by accounting for (i) the solution chemistry of oxalate, (ii) the solubility product of calcium oxalate monohydrate, (iii) material balances for total oxalate and calcium concentrations, and (iv) charge electroneutrality. The equations used in this model are presented below. The solubility product, K_{sp} , is defined as,

$$K_{sp} = [Ca^{2+}][C_2O_4^{2-}]. \quad (3-2)$$

Oxalate (or oxalic acid) is a diacid with two dissociation constants:

$$K_{a1} = \frac{[HC_2O_4^-][H^+]}{[H_2C_2O_4]} \text{ and} \quad (3-3)$$

$$K_{a2} = \frac{[C_2O_4^{2-}][H^+]}{[HC_2O_4^-]}. \quad (3-4)$$

Since all reactions take place in aqueous solutions, we must account for the water dissociation constant,

$$K_w = [H^+][OH^-]. \quad (3-5)$$

Moreover, the overall charge of electrolyte solution is neutral,

$$0 = 2[Ca^{2+}] + [H^+] - [OH^-] - [HC_2O_4^-] - 2[C_2O_4^{2-}] + [Na^+] - [Cl^-]. \quad (3-6)$$

The total concentration of calcium ions in solution equals the calcium ions in COM crystals and the free calcium ions in solution,

$$[Ca^{2+}]_{total} = [Ca]_{COM} + [Ca^{2+}], \quad (3-7)$$

The mass balance for the total oxalate concentration accounts for the fully protonated form, $H_2C_2O_4$, which is present in trace quantity at physiological pH, the dissociated forms of free oxalate in solution, and the concentration within COM crystals:

$$[Ox^{2-}]_{total} = [Ox]_{COM} + [C_2O_4^{2-}] + [HC_2O_4^-] + [H_2C_2O_4]. \quad (3-8)$$

COM crystallization was performed with an equimolar ratio of calcium and oxalate,

$$[Ca^{2+}]_{total} = [Ox^{2-}]_{total}. \quad (3-9)$$

The electroneutrality relationship (Eq. 3-6) was simplified by expressing the concentration of free calcium ions with solubility product, Eq. 3-2, and the concentration of free oxalate ions by the substitution of Eqs. 3-3 and 3-4,

$$0 = [H^+] + 2 \frac{K_{sp}[H^+]^2}{K_{a1}K_{a2}[H_2C_2O_4]} - \frac{K_w}{[H^+]} - K_{a1} \frac{[H_2C_2O_4]}{[H^+]} - 2K_{a1}K_{a2} \frac{[H_2C_2O_4]}{[H^+]^2} + [Na^+] - [Cl^-], \quad (3-10)$$

Further simplification of Eq. 3-9 was achieved by the substitution of Eqs. 3-7 and 3-8,

$$0 = [H_2C_2O_4] - \frac{K_{sp}[H^+]^2}{K_{a1}K_{a2}[H_2C_2O_4]} + K_{a1} \frac{[H_2C_2O_4]}{[H^+]} + K_{a1}K_{a2} \frac{[H_2C_2O_4]}{[H^+]^2}. \quad (3-11)$$

The simplified Eqs. 3-10 and 3-11 possess only two unknown variables: the concentration of hydrogen ions and oxalic acid. The dissociation constants and solubility product were taken from literature [24] and concentrations of sodium ion and chloride were input variables. The nonlinear series of equations was solved by solver using Matlab for a range of pH, as shown in Figure 3-5. Figure 3-5A shows the change of calcium ion concentration in the solution; experimental values are marked with a cross and theoretical values are in solid lines. The calcium ion concentration sharply decreases in $pH < 5$ and in $pH > 6$ the concentration of calcium ion stays constant regardless of pH. Figure 3-5B represents the concentration of three oxalate species in the pH range $3 < pH < 11$. The concentration of $H_2C_2O_4$ is almost non-existent (recall $pK_{a,1} = 1.23$) and as pH increases to 5 the concentration of $HC_2O_4^-$ decreases (recall $pK_{a,2} = 4.19$) while the concentration of $C_2O_4^{2-}$ increases to a certain concentration. The apparent change in solubility of COM crystals in $pH < 5$ is due to the dissociation of oxalate i.e., the pH should be greater than 5 for oxalate to be fully dissociated. Theoretically, the solubility of COM crystals does not change with pH

which is consistent with past studies done by others [66]. The discrepancy between experimental values and calculated values is likely due to the fact that we did not account for activity coefficients in the calculations. Activity coefficients can be calculated based on the Davies equation,

$$\log(\gamma) = -0.5 z^2 \left(\frac{\sqrt{I}}{1+\sqrt{I}} - 0.2I \right), \quad (3-12)$$

where z is the charge of ion and I is the ionic strength. Future analysis will incorporate the activity coefficients, which will require numerical methods. The calculated solubility is expected to increase closer to the experimental values once the activity coefficients are taken into consideration.

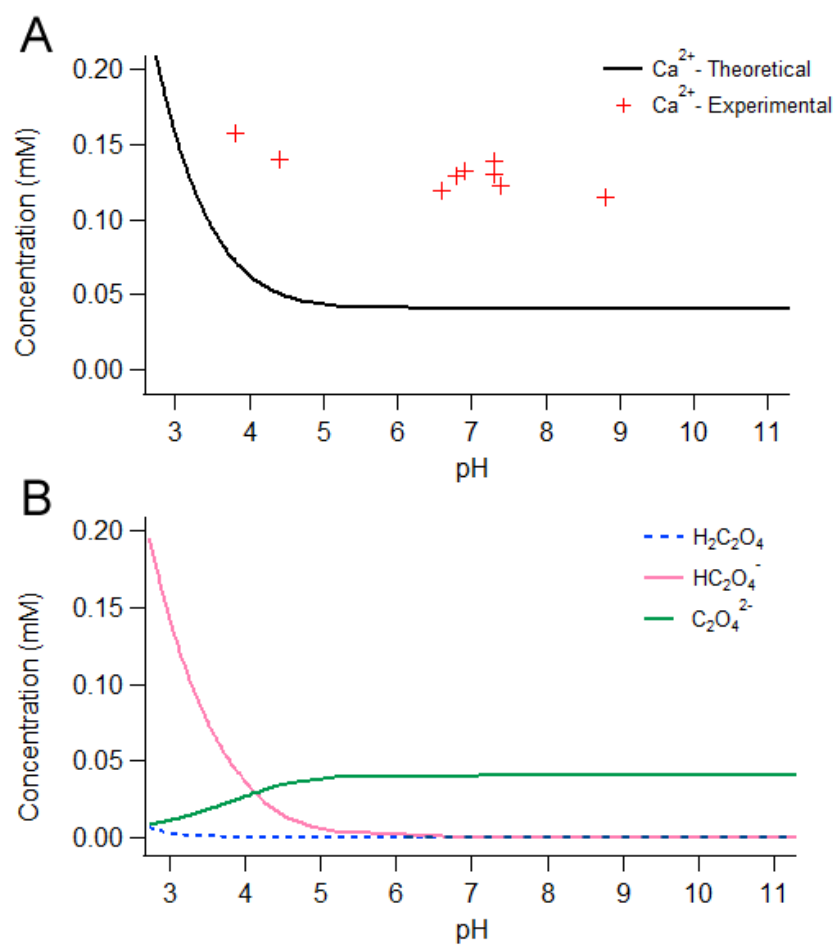


Figure 3-5. Solubility COM crystals of both experimental and calculated values. (A) The concentration of free calcium ions as a function of pH for experimental (symbols) and theoretical (line). (B) The theoretical concentrations of three oxalate species.

4. Molecular Analogues of Citrate

There have been tremendous amount of research on calcium carbonate which is a biomineral present in the shells of marine organisms. These shells consist of a crystalline inorganic phase within a polymeric organic matrix. It is believed that this association between the inorganic minerals and the organic macromolecules is the key to elucidate such elegantly controlled structures. The organic macromolecules seem to possess the ability to regulate the assembly of minerals and ultimately regulate the nucleation, growth, morphology and the polymorphic structure of the minerals. Calcium carbonate exists in three different polymorphs: calcite (the most thermodynamically stable form, aragonite and vaterite [19]. In attempts to direct the growth of calcite, people have studied the role of organic molecules present in biominerals and found out these molecules contained acidic matrix proteins or glycoproteins [17]. There have been many efforts to mimic the influence of these matrix proteins by observing the effect of acidic polypeptides [70, 71] such as polyaspartic acid [18] and other polyanions [11, 72] and proteins extracted from the nacre [73, 74] and shell of exoskeleton [75]. The past work on biominerals motivates the investigation of urinary components and their derivatives or structural analogues.

4.1 Structural mapping of organic growth modifiers

The inspiration to investigate organic growth modifiers in this study came from the preliminary studies of our collaborator, Dr. John Asplin. Studies by Asplin and coworkers compared the efficacy of two molecules, citrate (CA) and hydroxycitrate (HCA). As previously discussed, CA is a common treatment for stone disease and a constituent often included in dietary calcium supplements. HCA is also

recognized by the FDA as an over-the-counter supplement that is commonly used for weight loss. Asplin used seeded COM crystal growth to compare the efficacy of CA and HCA. Seed crystals were added to a metastable COM growth solution in the presence of CA or HCA and in the absence of inhibitors. Addition of seed crystals triggered the consumption of oxalate ions, which was continuously recorded using a spectrophotometer at 214 nm for 420 seconds. Three different concentrations of CA and HCA were studied and it was observed that the percent inhibition of HCA was higher than that of CA at all three concentrations. Moreover, it was observed that the percent inhibition increased for both CA and HCA with increased inhibitor concentration. In order for a COM crystal inhibitor to be an effective therapeutic for nephrolithiasis, it needs to be excreted in urine.

To this end, Asplin conducted a preliminary experiment with a single normal subject on urinary concentration of HCA after oral intake. Urine specimens were collected over an eight hour period, at two hour increments, and it was shown that the concentration of HCA peaked within a two to four hour period. This result was in good agreement with the data presented by Loe et al. where Loe and coworkers examined the concentration of HCA in blood of four subjects after oral intake of HCA and found that the concentration of HCA also peaked at two hours [12]. Hence, these preliminary results suggest that HCA may serve as an effective inhibitor for COM crystal growth *in vivo*. An interesting finding from these studies is that a subtle difference in structure between CA and HCA (i.e., one additional hydroxyl group) results in dramatic changes in percent inhibition of COM crystallization. This observation motivates a more rigorous investigation of the role of functional groups, notably the number and spatial positioning of carboxyl and hydroxyl groups, on both

the specificity and efficacy of OGMs. To this end, we composed a structural map of organic growth modifiers (Figure 4-1) to systematically investigate structural modifications to oxalate through a series of steps to progressively approach CA and HCA.

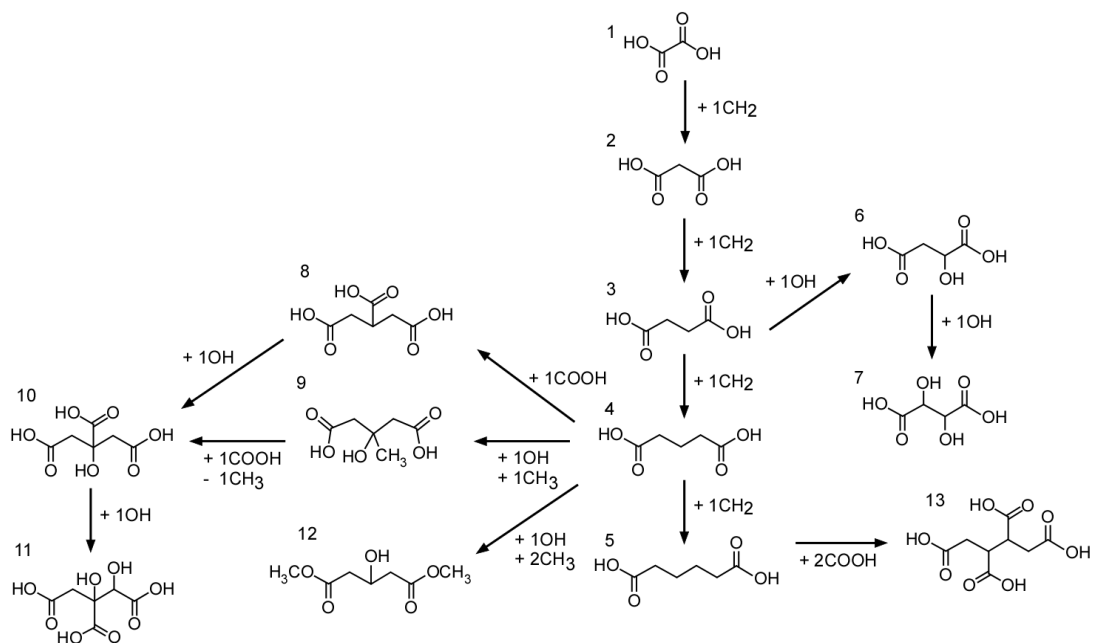


Figure 4-1. Structural mapping of the OGMs used in this study, which include: 1-oxalic acid, 2-malonic acid, 3-succinic acid, 4-glutaric acid, 5-adipic acid, 6-malic acid, 7-tartaric acid, 8-tricarballic acid, 9-hydroxy methylglutaric acid, 10-citric acid, 11-hydroxycitric acid, 12-dimethyl hydroxyglutaric acid, 13-butanetetracarboxylic acid.

The names and corresponding abbreviations of the chemicals tested as OGMs in this study are as follows: 1-oxalic acid (OA), 2-malonic acid (MA), 3-succinic acid (SA), 4-glutaric acid (GA), 5-adipic acid (AA), 6-malic acid (MAL), 7-tartaric acid (TTA), 8-tricarballic acid (TCA), 9-hydroxy methylglutaric acid (HMGA), 10-citric acid (CA), 11-hydroxycitric acid (HCA), 12-dimethyl hydroxyglutaric acid (DHG), 13-butanetetracarboxylic acid (BTCA). We designed the set of OGMs starting from OA, which is a constituent of COM crystals. The inhibitor CA is derived from OA via

the addition of three aliphatic backbone carbons (e.g., GA), the addition of one carboxyl group (e.g., TCA), and the addition of one hydroxyl group. Incorporation of one more hydroxyl group yields HCA, which is a stronger inhibitor than CA. With this logic, the effects of functional groups on COM crystallization were examined by systematically adding or removing groups from either CA or HCA to examine the effects of functional moieties and spatial patterning of these groups in selected OGMs. Two general aspects were observed: (i) The effect of an additional hydroxyl group, which was examined by comparing (1) TCA, CA and HCA, (2) GA and DHG, and (3) SA, MAL and TTA; and (ii) the impact of carboxyl groups, which was observed by comparing (1) GA and TCA, (2) MAL and CA, and (3) TTA and HCA.

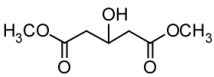
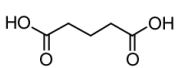
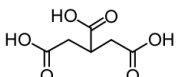
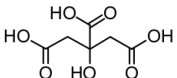
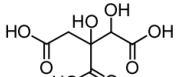
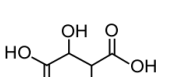
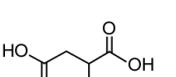
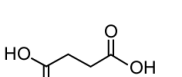
4.2 Effect of organic growth modifiers on COM crystallization

The effect of OGMs on COM crystallization was assessed by comparing the size and aspect ratio of crystals prepared in the absence (control) and in the presence of OGMs. COM crystals in the presence of OGMs were prepared with 60 $\mu\text{g/mL}$ of each modifier. The pH change resulting from the addition of acidic OGMs was corrected by the appropriate addition of stock $\text{NaOH}_{(\text{aq})}$ solution to achieve a desired pH equal to the control (i.e., pH 6.2). The aspect ratio of COM crystals is shown in Figure 4-2A and the [001] length of the crystals is provided in Figure 4-2B. These studies revealed that the majority of OGMs have a marginal effect on the aspect ratio of crystals relative to the control, with the exception of CA and HCA. When we compare crystals prepared with different OGMs, there are apparent trends. First, increasing the number of hydroxyl groups in OGMs with a C_5 backbone decreases the aspect ratio while it is not always the case for OGMs with a C_4 backbone. For

instance, when comparing DHG and GA where the former has one additional hydroxyl group, the aspect ratio of DHG is 17% lower. Comparing TCA and CA, the additional hydroxyl group of CA yields a 20% reduction in the aspect ratio. Also in the case of CA and HCA (where HCA has one additional hydroxyl group), the aspect ratio of HCA is 33% lower. A comparison of MAL and SA (which has one less carbon in its backbone than GA) reveals that the aspect ratio of SA is 18% higher whereas when we compare MAL and TTA (where TTA has one additional hydroxyl group), the aspect ratio of TTA is 8% lower.

A second observed trend is that additional carboxyl groups decrease the aspect ratio of crystals. For instance, the aspect ratio of TCA is 8% lower than GA (which has one less carboxyl group). Sheng et al. studied the influence of citrate on the adhesion between a modified AFM tip and COM surfaces using AFM [4]. They measured the adhesion force between a gold probe functionalized with thiols containing carboxyl terminal groups and the three COM surfaces, (100), (010) and (12-1), in the presence of citrate. The adhesion force between the tip and crystal surface decreased with increasing citrate concentration for all three faces, which indicated that citrate suppressed the adhesion between COM crystal faces and the probe (i.e., a setup that generically mimics interactions that are encountered *in vivo* between COM crystal and renal epithelial cells). Sheng et al. also conducted a parallel experiment in the presence of propionate, which is a simple monocarboxylic acid ($\text{C}_2\text{H}_5\text{COOH}$), and found that the monocarboxyl group was not as effective in suppressing the adhesion as tricarboxyl group. This result supports the important role of multiple carboxyl groups as OGM moieties for inhibiting COM crystallization.

Table 4-1. List of OGM structures and their effect on the aspect ratio and the length of COM crystals.

| Name | Structure | Aspect ratio, [001]/[010] | [001] length (μm) |
|------|---|---------------------------|--------------------------------|
| DHG |  | 2.5 ± 0.5 | 35 ± 7 |
| GA |  | 3.0 ± 0.6 | 68 ± 16 |
| TCA |  | 2.7 ± 0.6 | 56 ± 13 |
| CA |  | 2.2 ± 0.2 | 72 ± 11 |
| HCA |  | 1.5 ± 0.1 | 34 ± 4 |
| TTA |  | 2.9 ± 0.5 | 46 ± 9 |
| MAL |  | 3.1 ± 0.6 | 73 ± 19 |
| SA |  | 2.6 ± 0.6 | 57 ± 16 |

These studies also revealed that an OGM's effect was more noticeable on the length of crystals than on the aspect ratio. All OGMs, except for HCA, increased the length of crystals with respect to the control by as much as 78% (e.g., MAL was the most efficient). The effect of OGMs on the [001] crystal length was also compared between different OGMs. First, the effect of hydroxyl groups was assessed. For instance, in the case of DHG and GA, the length of crystals was 48% lower for DHG

compared to GA, whereas for MAL, SA, and TTA, the length increased by 28% using SA and decreased by 37% using TTA compared to MAL. An additional effect was the role of carboxyl groups. In the case of GA and TCA, the COM crystal length decreased by 17% using TCA compared to GA, whereas the crystal length increased by 29% using TCA and decreased by 53% using HCA relative to the [001] crystal length in the presence of CA.

The structural difference between SA (C_4) and GA (C_5) is the length of their carbon backbone, which differ by one carbon. The number of carbons along the OGM backbone alters the flexibility of the molecule and also the ability of carboxyl functional groups to bind to surface sites on COM crystals. This can explain the different trends in aspect ratios observed for the OGMs in Figure 4-1. The molecular recognition of these OGMs for different crystal faces of COM is also determined by the topology of the three crystallographically planes – the (100), (010), and {12-1} faces – of COM crystals. Figure 4-3A contains the views of the COM crystal structure normal to each crystal plane, while Figure 4-3B represents the views parallel to the plane (i.e., 90-degree rotation of each image in Figure 4-3A).

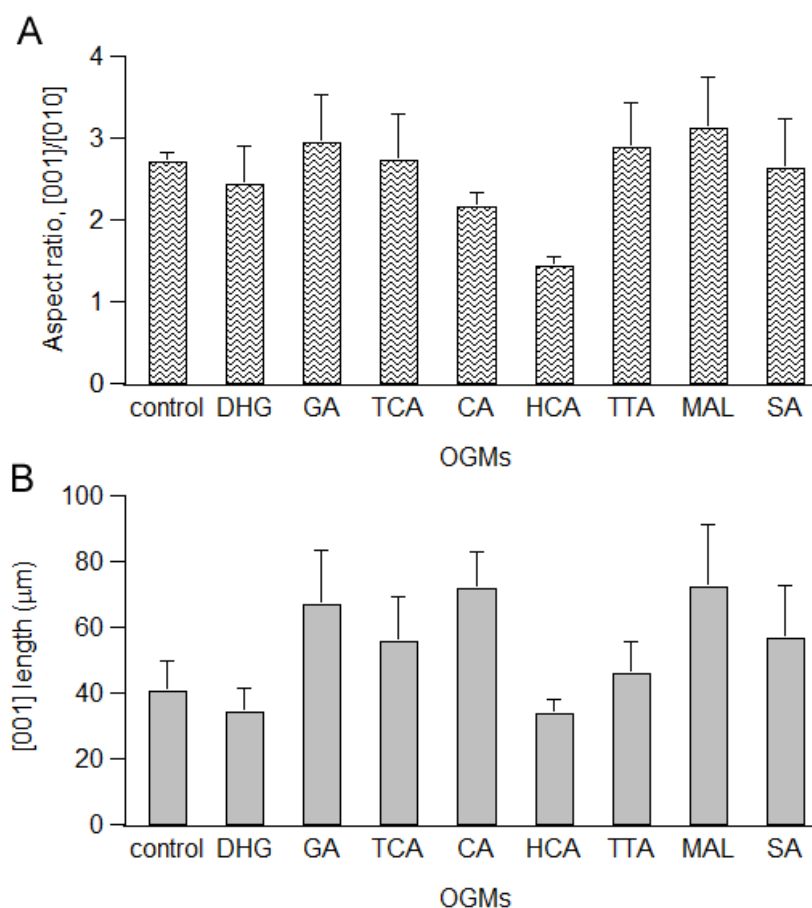


Figure 4-2. Effect of selected OGMs on COM crystallization. (A) The bar graph shows the length-to-width aspect ratio (or [001]/[010]) of COM crystals as a function of different OGMs. (B) The bar graph shows the average length (or [001] dimension) of COM crystals. All measurements were done with ca. 70 crystals from one batch except for control which was done with five different batches. Error bars equal one standard deviation.

The carboxylate groups of OGMs can bind to oxalate vacancies in the COM crystal surface via the formation of a calcium bridge, $\text{-COO}^-_{(\text{OGM})} \dots \text{Ca}^{2+} \dots \text{OOC}^-_{(\text{COM})}$. According to Figure 4-3B, the orientation of oxalate molecules and/or the carboxyl group of a modifier that binds to each plane is different. For instance, modifiers bind to the (010) plane with its carboxyl group perpendicular to the plane ($\Theta = 90^\circ$), whereas modifiers bind to the (100) or {12-1} surfaces with different angles ($\Theta < 90^\circ$). For instance, the decrease in aspect ratio from GA to DHG indicates that the DHG is

preferentially interacting with the $\{12-1\}$ surfaces. Conversely, the increase in aspect ratio from SA to MAL suggests a preferential binding of MAL to the (010) surface. In addition, crystals prepared in the presence of TCA, CA, and HCA exhibit a continuously decreasing aspect ratio as more hydroxyl groups are added to the OGM molecules. It appears that the additional hydroxyl groups facilitates the preferential binding of OGMs to specific crystal surfaces, possibly due to the formation of hydrogen bonds between the modifiers and crystal surface.

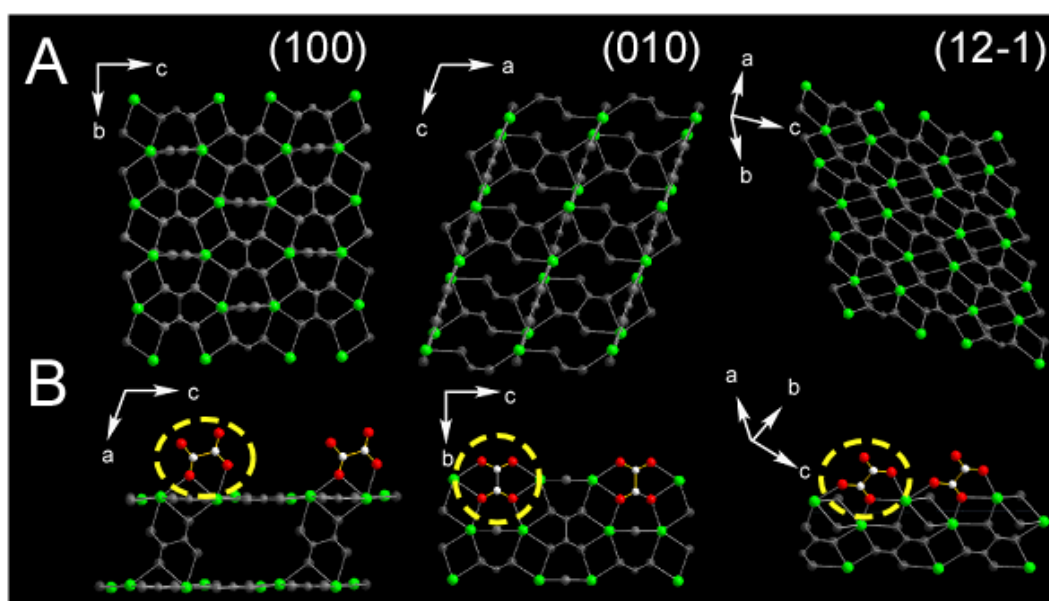


Figure 4-3. Molecular topology of three crystallographically significant planes of calcium oxalate monohydrate: (100), (010) and (12-1). (A) Structures viewed normal to the plane, and (B) a side profile viewed along the plane. Note the different orientation of oxalate molecules in each plane (dashed circles).

4.3 Efficacy of organic growth modifiers

The efficacy of OGMs was examined using the ISE method discussed in Ch. 2 to monitor the temporal depletion of free calcium ions in solution (reported in this study as the rate of growth, or slope of ISE curves, with unit in ppm/min). The percent

inhibition of OGMs is shown in Figure 4-4, which compares the growth rate of OGMs to that of the control (without any modifiers). All OGMs had some inhibitory effect on COM crystallization (as represented by the percent reduction relative to the control).

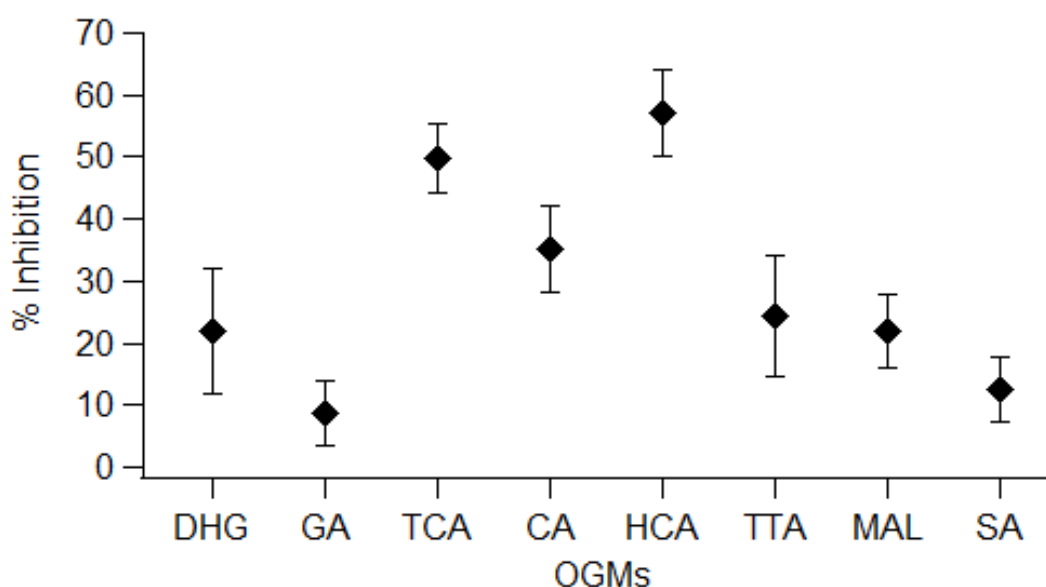


Figure 4-4. Percent inhibition of selected OGMs on COM crystallization at 25°C as measured *in situ* using a calcium ion-selective electrode. Data were averaged from at least five different measurements. Error bars equal two standard deviations.

In the case of DHG and GA, the percent inhibition of the former was nearly 1.5 times higher than that of GA. A comparison of OGMs with increasing number of hydroxyl groups (i.e., TTA > MAL > SA) revealed that the percent inhibition of TTA was 10% higher than that of MAL, which in turn exhibited a percent inhibition that was 74% higher than that of SA. This demonstrates the enhanced inhibitory effect that occurs by the addition of hydroxyl groups. However, this trend is less evident when comparing TCA, CA, and HCA. For instance, the addition of one hydroxyl group from TCA to CA resulted in a 29% reduced percent inhibition. Furthermore, the

addition of one more hydroxyl group from CA to HCA resulted in a 62% increase in the percent inhibition. Collectively, these results suggest that hydroxyl groups can enhance the OGM efficacy, but are not the sole contributors of a molecule's ability to inhibit COM growth.

These results also suggest that the introduction of hydroxyl groups may introduce steric hindrance when modifiers bind to crystal surfaces. Moreover, it was interesting to observe that all three carboxyl groups contribute to the OGM inhibitory effects. For instance, there was a sharp (nearly 5-fold) increase in percent inhibition from GA to TCA, where the latter has one additional carboxyl group. Likewise, comparisons of (i) CA and MAL and (ii) HCA and TTA revealed that OGMs with a larger number of carboxyl groups (i.e., CA and HCA) were higher efficacy growth inhibitors of COM crystallization. In order to examine OGM binding to COM surfaces to elucidate their mode of action at a molecular level, one would need to combine these bulk crystallization studies with molecular simulations (a topic outside the scope of this work). Nevertheless, these results clearly indicate the important roles of carboxyl and hydroxyl functional moieties in high efficacy OGMs.

4.4 Potency studies

Potency studies were performed with selected OGMs to examine their influence on COM crystallization (i.e., crystal aspect ratio) as a function of OGM concentration. The modifiers TCA, CA, and HCA were selected to further examine their potency since these OGMs were the most effective inhibitors (based on studies in section 4.3). Potency studies were performed at five different concentrations: 1, 5, 10, 20, and 60 $\mu\text{g/mL}$. The effect of OGMs at different concentrations on the aspect ratio of crystals is shown in Figure 4-5A. The modifier TCA showed marginal effect

on the aspect ratio of COM crystals at all concentrations, 1 to 60 $\mu\text{g/mL}$. Likewise, CA had little effect on the aspect ratio at concentrations between 1 and 20 $\mu\text{g/mL}$; however, at 60 $\mu\text{g/mL}$ CA our studies revealed a 20% reduction in COM crystal aspect ratio compared to the control. In the case of HCA, the aspect ratio of COM crystals decreased with increasing concentration of HCA in a linear fashion when compared to the control. At concentrations of 1, 5, 10, 20 and 60 $\mu\text{g/mL}$ HCA, the percent reduction in aspect ratio was 10, 14, 25, 35, and 46%, respectively. As such, it appears that the interaction between TCA and COM crystal surfaces are non-specific (i.e., TCA binds to any of the three faces without any preferences). In the case of CA and HCA, both modifiers decreased the COM crystal aspect ratio, which indicates a preferential binding of CA and HCA to the $\{12-1\}$ surface. A comparison of results in Figure 4-5 reveals that HCA is more potent than CA.

The effect of OGMs at different concentrations on the $[001]$ length of COM crystals is shown in Figure 4-5A. In most cases, there was not a strong concentration-dependence. For instance, in the presence TCA at concentrations between 1 and 20 $\mu\text{g/L}$, there was only a 15 to 20% reduction in the length of crystals compared to the control; and in the presence of TCA at 60 $\mu\text{g/mL}$, the $[001]$ length of COM crystals was increased by 38% compared to the control. COM crystallization in the presence of CA at concentrations of 10 and 20 $\mu\text{g/mL}$ revealed a ca. 15% increase in $[001]$ dimension, while higher concentrations (i.e., 60 $\mu\text{g/mL}$) resulted in a 78% increase in COM crystal length compared to the control. Since the aspect ratio did not reveal much change between OGMs and the control, the increase in COM $[001]$ crystal length indicates the formation of larger crystals, which is potentially attributed to inhibited nucleation of crystals. In the case of HCA, most concentrations resulted in a

reduction in the length of crystals (as much as 18%), except for 5 $\mu\text{g/mL}$ where the length of crystals increased by 24% compared to the control. Further studies are required to ascertain if this effect is attributed to experimental error.

Optical micrographs of COM crystals prepared with different concentration of CA and HCA are shown in Figure 4-6. Three concentrations (10, 20 and 60 $\mu\text{g/mL}$) are shown to observe the effects of OGMs on COM crystals since concentrations of 1 and 5 $\mu\text{g/mL}$ did not markedly alter COM crystal habit. It can be clearly seen that increasing the concentration of CA results in the reduction of crystal aspect ratio and the rounding of apical points. This rounding of crystal edges is consistent with past observations [76, 77], and is attributed to the preferential binding of citrate to $\{12-1\}$ faces; however, others have reported rounding in all $\{12-1\}$ faces of the apical tips. In this study there were COM crystals with equal rounding, but most crystals exhibited rounding on one-side resulting in teardrop-shape crystals (Figure 4-6D). In the case of HCA, the reduction in the aspect ratio of crystals is more dramatic than that of CA at the same concentration. The rounding of edges can also be observed with HCA at 20 and 60 $\mu\text{g/mL}$.

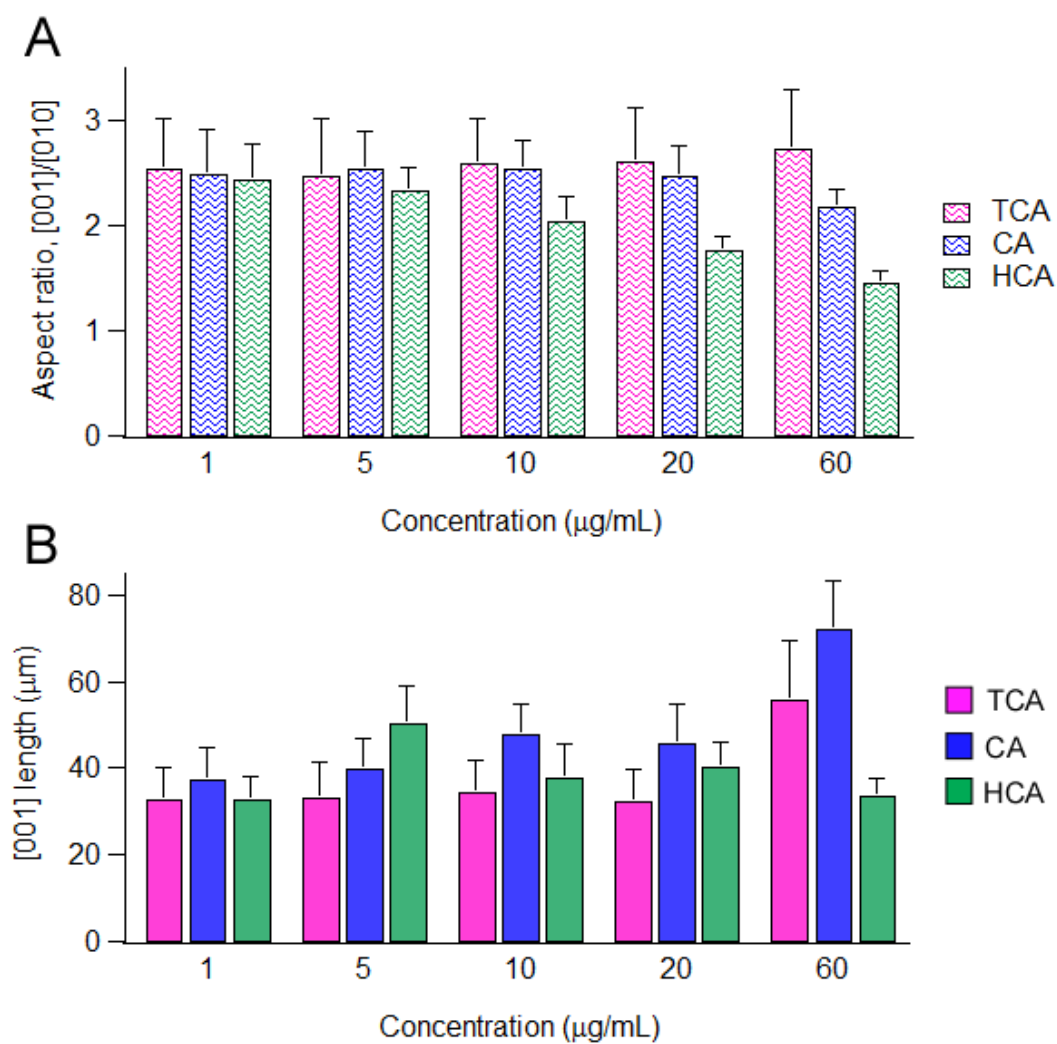


Figure 4-5. Aspect ratio (A) and $[001]$ length (B) of COM crystals prepared with different concentrations of TCA, CA, and HCA. Concentrations used for this study were 0, 1, 5, 10, 20 and 60 $\mu\text{g/mL}$. Each measurement was done from ca. 70 crystals. Error bars equal one standard deviation.

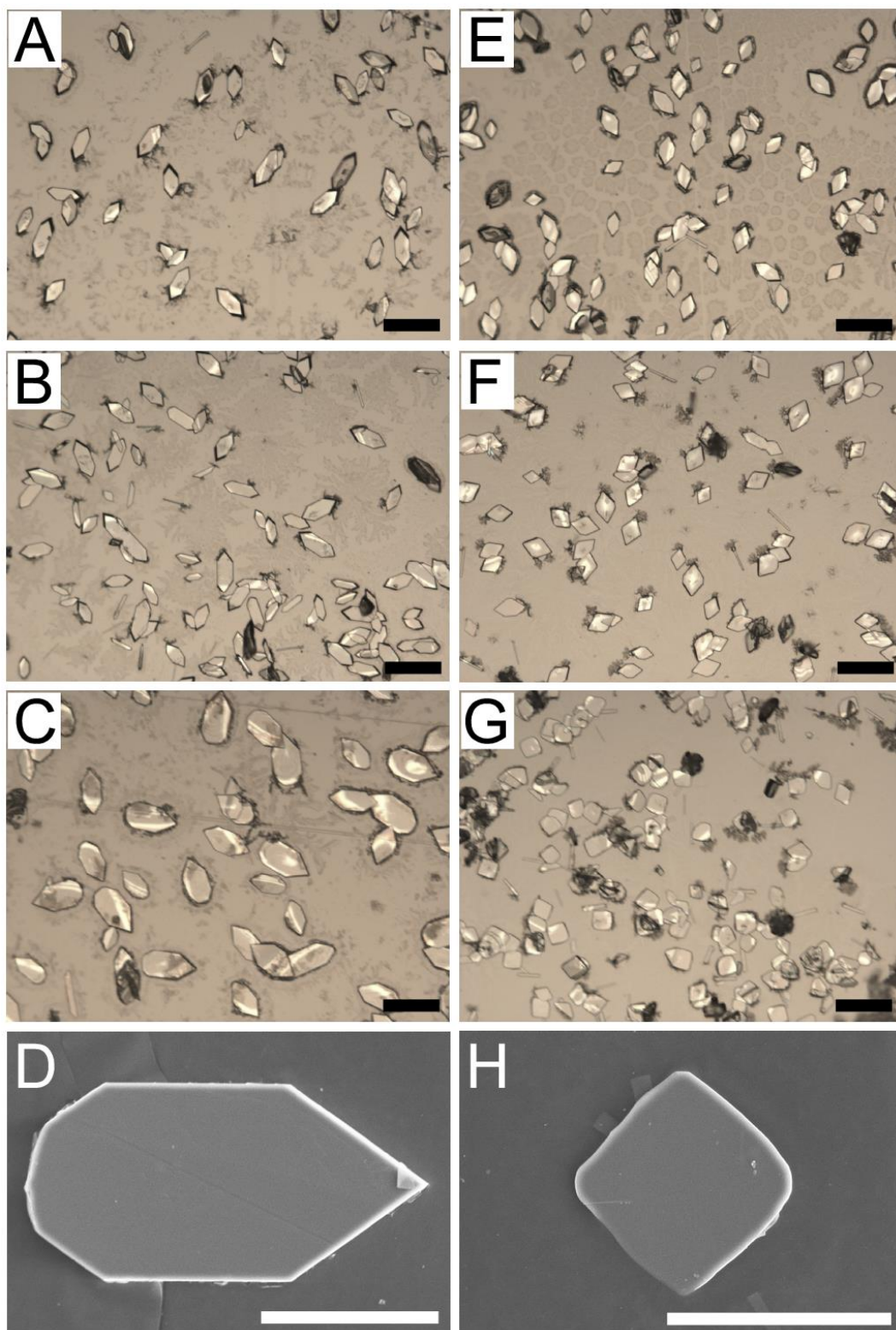


Figure 4-6. Optical micrographs of crystals prepared with CA at 10 $\mu\text{g/mL}$ (A), 20 $\mu\text{g/mL}$ (B), 60 $\mu\text{g/mL}$ (C), and crystals prepared with HCA at 10 $\mu\text{g/mL}$ (E), 20 $\mu\text{g/mL}$ (F), 60 $\mu\text{g/mL}$ (G). Scanning electron micrographs of crystals with 60 $\mu\text{g/mL}$ -CA (D) and 60 $\mu\text{g/mL}$ -HCA (H) are shown. All scale bars indicate 30 μm .

The efficacy of TCA, CA, and HCA on COM crystallization at five different concentrations was examined using ISE measurements (as discussed in Ch.2). The results are shown in Figure 4-7. There was a concentration dependence yielding a trend of increasing percent inhibition with increasing concentration of OGMs. For instance, TCA at the concentration range of 1 to 5 $\mu\text{g/mL}$ promoted the growth of COM crystals; however, at 60 $\mu\text{g/mL}$ TCA exhibited a 41% inhibition of COM crystal growth, which is slightly higher than that of CA, a reportedly moderate inhibitor. TCA at low concentration could have been considered as impurity due to its non-specific binding and it could have been incorporated into the crystal growth; however, further studies are required to exclude any experimental errors. In the case of CA, the percent inhibition of crystal growth increased with increasing modifier concentration; however, the effect appears to level off at relatively lower concentration compared to TCA and HCA (i.e., comparing concentrations from 20 to 60 $\mu\text{g/mL}$, the percent inhibition of CA was increased by 33% whereas the percent inhibition of TCA and HCA were increased by 200% and 50%, respectively). As was anticipated from bulk crystallization studies, HCA proved to be the most potent inhibitor of COM crystal growth, as evidenced by the large increase in percent inhibition with increasing concentration, and the gradual leveling off at a concentration of ca. 60 $\mu\text{g/mL}$.

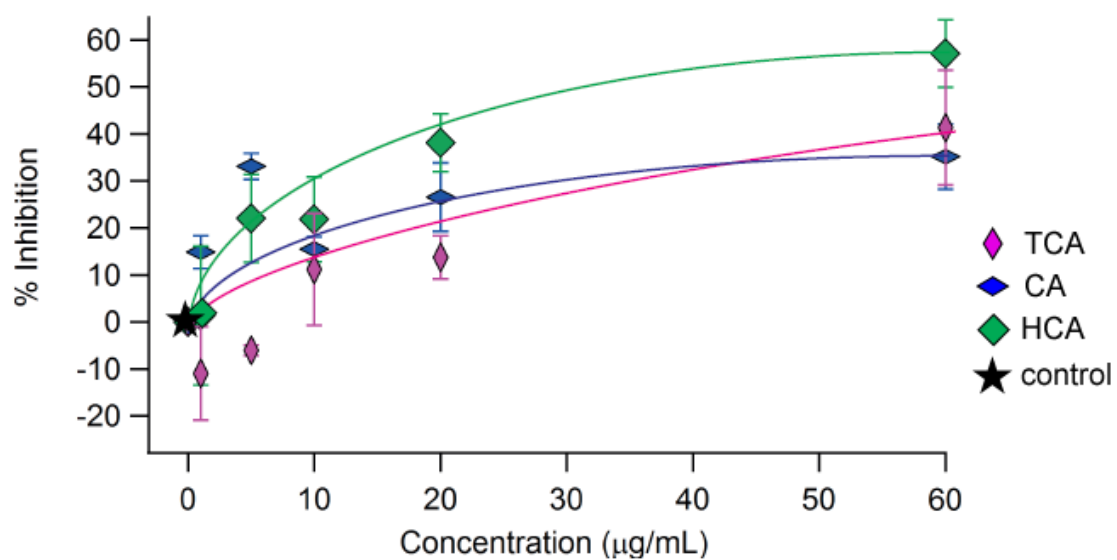


Figure 4-7. Percent inhibition of crystals prepared with different concentrations of TCA, CA, and HCA. The following concentrations of OGM were examined: 0, 1, 5, 10, 20, and 60 $\mu\text{g/mL}$. Error bars equal two standard deviations and lines are interpolations of the data.

5. Design of Tailored Peptides

Previous chapters have focused on the characterization of small organic modifiers as inhibitors of COM crystallization; however, it is well documented that larger macromolecules tend to be more effective inhibitors relative to smaller molecules. For instance, Ward and coworkers showed that polyamino acids (5 – 15 kDa) are nearly 1000 times more potent than their corresponding amino acids [55, 78]. Likewise, DeYoreo and coworkers showed that urinary proteins, such as osteopontin, are significantly more effective inhibitors of COM growth relative to citrate [79, 80]. Along these lines, future initiatives to develop potential drugs for COM kidney stone disease will focus on the design and testing of larger macromolecules.

Peptides are an attractive template for designing tailored growth inhibitors since the modular synthesis of peptides is easy to manage for high-throughput analyses. The sequence of peptides can be modified with different size, sequence, and secondary structure; also the residues can be easily substituted to alter peptide functionality. They are also suitable templates for modifying physicochemical properties critical for drug delivery, which include solubility, bioavailability, and toxicity. High-throughput methods enable rapid synthesis and screening of peptide libraries, which can otherwise be challenging due to the variable number of sequences that can be constructed from different amino acids. To rationally design inhibitors, it is imperative to judiciously select inhibitors with appropriate functionality, size, and structure that can be tuned at a molecular level to recognize a specific crystal surface. For instance, an extensive study of an 18-mer peptide using all natural amino acids

would be virtually impossible. An exhaustive study of all unique 18-mer sequences derived from a library of only two amino acids (e.g., L-Asp and L-Ala) would require screening a smaller, but still substantially large, library of more than 10^5 peptides. A more rational approach would be to start the peptide design using the selected sequences from known protein inhibitors of COM crystallization. For instance, the segment of osteopontin (OPN), which is one of the urinary constituents with abundant sequence domain rich in carboxylic acids, was studied by several groups [4, 24, 33, 40, 79, 80]. DeYoreo and coworkers examined COM growth in the presence of 27-mer peptides with repeating DDDX sequences (where D = Asp binding group and X = Ser or Gly spacer groups) and reported a 90% reduction in COM growth using peptide concentrations of 0.02 $\mu\text{g/mL}$ (X = Gly) and 2.2 $\mu\text{g/mL}$ (X = Ser). They reported that a 30-fold increase in peptide potency was achieved by simply switching the spacer from glycine (R group = H) to serine (R group = CH_2OH) [24].

In our studies, we selected L-aspartic acid (L-Asp) as a binder moiety since calcium-binding proteins tend to be rich in L-Asp . As a spacer (i.e., amino acid separating binder groups), we selected L-alanine (L-Ala). The binder is not the only functional group that can affect the interaction between peptides and COM crystals; the spacer groups can also play crucial role in COM growth inhibition. Ala was a desirable choice for the spacer due to its small side group ($\text{R} = \text{CH}_3$) where steric hindrance of binder interacting with COM crystal can be minimized. Also, the hydrophobic nature of Ala residue may facilitate the interaction between peptide and COM crystals through entropic effects where formerly oriented water molecules near the methyl group are released as Ala orients on COM crystal surfaces. Such entropic

effects have been proposed as a mechanism for inhibition of ice crystallization with antifreeze proteins in cold weather species [81-83].

5.1 High-throughput peptide synthesis

The peptide sequences selected for these studies (named D1–D13) are listed in Table 5-1, which represent combinations of randomly selected Ala and Asp sequences. Some of these peptides possess similar patterns with subtle changes such as the removal or addition of a single binder or spacer group (i.e., XDX, XDDX and XDDDX), which mimics patterns observed in the primary amino acid sequences of many calcium-binding proteins. This library was used as an initial test for our design approach to synthesize and screen effective inhibitors of COM crystallization. Peptides were synthesized by the Karande Lab (Rensselaer Polytechnic Institute) on an automated peptide synthesizer (Multipep RS, Intavis Inc., Germany). A detailed method can be found in the paper by Farmanesh et al. published in the *Journal of Crystal Growth* [84].

Table 5-1. List of peptide sequences used in this study.

| | 1 | 2 | 3 | 4 | 5 | 6 | 7 | 8 | 9 | 10 | 11 | 12 | 13 | 14 | 15 | 16 | 17 | 18 |
|-----|----------|----------|----------|----------|----------|----------|----------|----------|----------|----------|----------|----------|----------|----------|----------|----------|----------|----------|
| D1 | <u>D</u> | <u>D</u> | <u>D</u> | A | A | A | A | A | <u>D</u> | <u>D</u> | <u>D</u> | A | A | A | A | A | <u>D</u> | <u>D</u> |
| D2 | A | A | <u>D</u> | A | A | A | A | A | <u>D</u> | <u>D</u> | A | A | A | A | <u>D</u> | A | A | A |
| D3 | A | <u>D</u> | A | A | A | <u>D</u> | A | A | <u>D</u> | A | A | <u>D</u> | <u>D</u> | A | A | <u>D</u> | A | A |
| D4 | A | <u>D</u> | A | A | <u>D</u> | A | A | <u>D</u> | A | A | <u>D</u> | A | A | <u>D</u> | A | A | <u>D</u> | A |
| D5 | A | <u>D</u> | A | A | <u>D</u> | <u>D</u> | A | A | <u>D</u> | A | A | <u>D</u> | <u>D</u> | A | A | A | A | A |
| D6 | A | <u>D</u> | A | A | A | <u>D</u> | <u>D</u> | <u>D</u> | A | A | A | <u>D</u> | A | A | A | <u>D</u> | <u>D</u> | <u>D</u> |
| D7 | A | <u>D</u> | A | A | A | <u>D</u> | <u>D</u> | A | A | A | A | A | A | A | A | <u>D</u> | A | A |
| D8 | A | <u>D</u> | A | A | A | <u>D</u> | <u>D</u> | A | A | A | <u>D</u> | A | A | A | A | <u>D</u> | A | A |
| D9 | A | <u>D</u> | A | A | A | <u>D</u> | <u>D</u> | A | A | A | <u>D</u> | A | A | A | <u>D</u> | <u>D</u> | A | A |
| D10 | A | <u>D</u> | A | A | <u>D</u> | A | A | A | <u>D</u> | A | A | <u>D</u> | <u>D</u> | A | A | <u>D</u> | A | A |
| D11 | A | <u>D</u> | A | A | <u>D</u> | <u>D</u> | A | A | A | A | A | A | <u>D</u> | A | A | <u>D</u> | A | A |
| D12 | A | <u>D</u> | <u>D</u> | A | A | <u>D</u> | A | A | <u>D</u> | A | A | <u>D</u> | <u>D</u> | A | A | <u>D</u> | <u>D</u> | A |
| D13 | A | <u>D</u> | A | <u>D</u> | A | <u>D</u> | A | <u>D</u> | A | <u>D</u> | A | <u>D</u> | A | <u>D</u> | A | <u>D</u> | A | <u>D</u> |

5.2 Effect of peptides on COM crystal habit

The effect of peptides on COM crystals was examined by comparing the size and the aspect ratio of crystals prepared in the absence and in the presence of peptides at the concentration of 20 µg/mL. Crystals collected after their synthesis in the presence of peptides seemed to be categorized into two groups: Hexagonal platelets (similar to control samples) and diamond platelets. Figure 5-1 shows the optical micrographs of collected crystals in the presence of different peptides. Figure 5-2A compares the [001]/[010] aspect ratio of the hexagonal shaped crystals, which showed

marginal change from the control (except for D4, which exhibited a ca. 20% increase relative to the control). The [001] length of crystals seemed to be affected by peptides D1 and D4, in particular, as shown in Figure 5-2B. Since the aspect ratio did not significantly change for these peptides, the elongation in length of crystals indicates the formation of larger crystals. The formation of diamond-shaped crystals is related to the specificity of peptide binding to COM {12-1} surfaces. Figure 5-2C compares the percentage of diamond and hexagonal COM crystals for the peptide library. All peptides produced diamond-shaped crystals, but the majority exhibited less than 20% diamonds in their total crystal population. Peptides D5 and D8 exhibited the largest populations of diamond-shaped crystals, which suggests that these peptides bind more effectively to COM {12-1} surfaces and inhibit growth normal to the [12-1] directions. The effect of doubling the concentration of peptide D8 (i.e., increasing the concentration from 20 to 40 $\mu\text{g/mL}$) was examined to confirm whether the relative percentage of diamond-shape crystals would increase; however, there was no appreciable increase in the population of diamond crystals.

Farmanesh et al. also examined the effect of this peptide library on the percent inhibition of COM crystallization. These studies revealed that the peptides exhibited a range of efficacy spanning 0 to 60% inhibition. In many cases, switching a single binder group position within the primary amino acid sequence led to dramatic changes in the peptide effectiveness as a growth inhibitor. This highlights how subtle changes in the inhibitor structure and/or functional composition can impact its molecular recognition for binding to different crystal surfaces. Interestingly, many of these randomly selected peptides outperformed citrate, which is considered a moderate inhibitor of COM crystallization. For instance, we previously showed that citrate

exhibits a 27% reduction in COM growth rate relative to the control (citrate at 20 $\mu\text{g/mL}$) – a value that is nearly half that of the most effective peptides in the D1-D13 library. It is also interesting to mention that the maximum percentage of diamond crystals observed among the peptides analyzed was ca. 34% compared to hydroxycitrate, a much smaller molecule, which converted more than 90% of hexagonal platelets to diamond-shaped crystals at the same concentrations tested for the peptides.

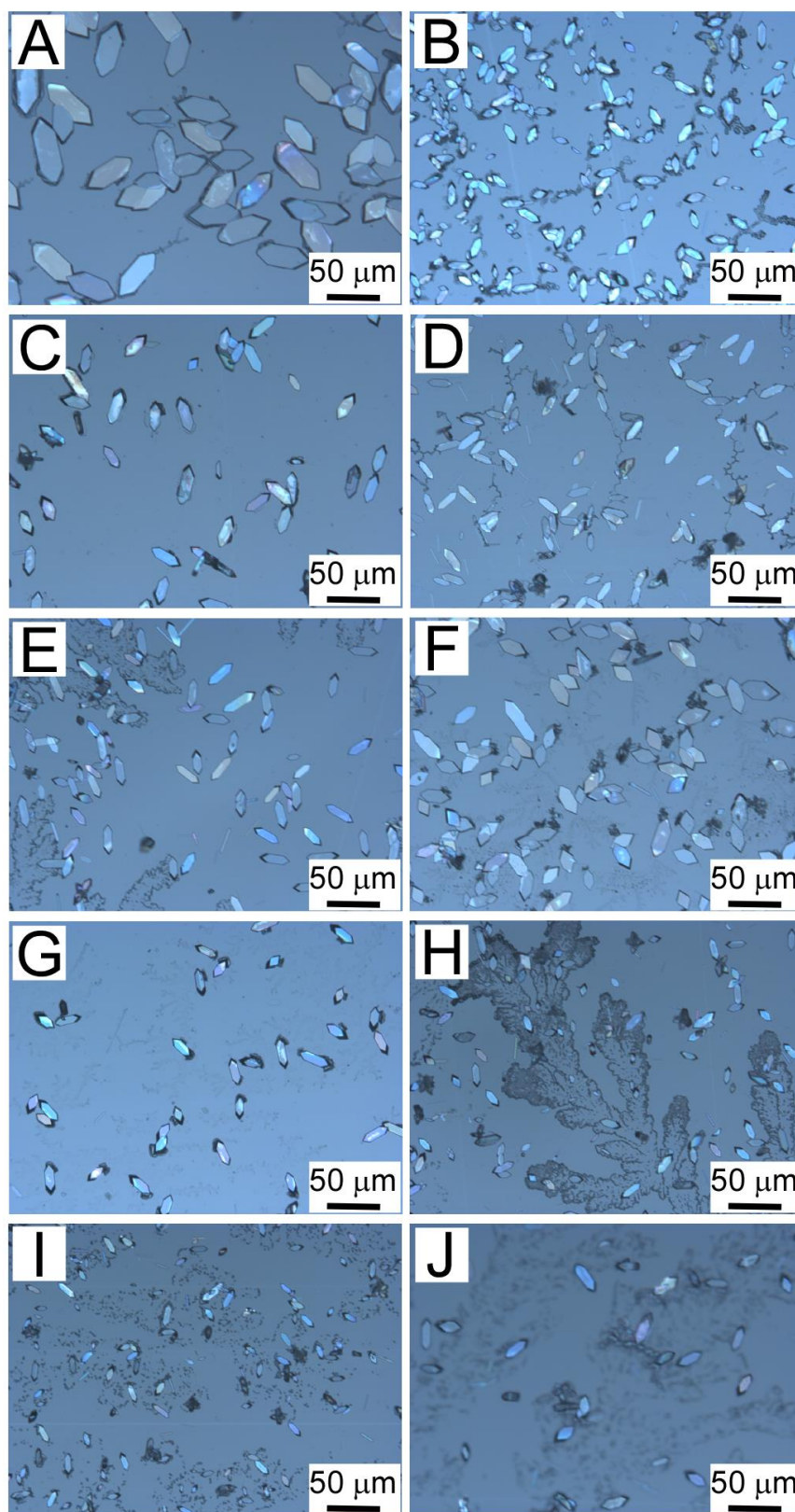


Figure 5-1. Optical micrographs of crystals prepared with different peptides. (A) D1; (B) D2; (C) D3; (D) D4; (E) D5; (F) D6; (G) D7; (H) D8; (I) D9; (J) D10. All images were taken under reflectance mode.

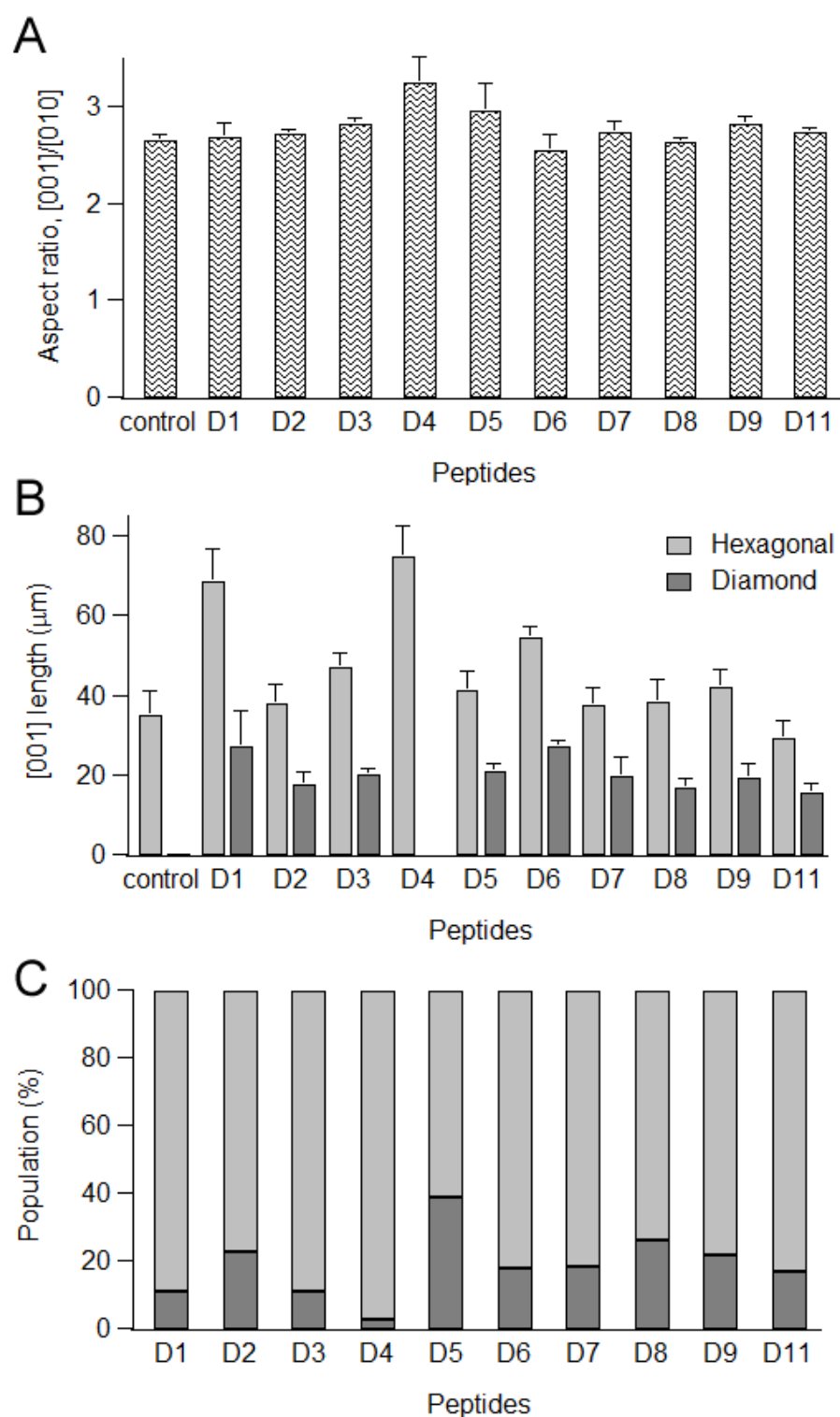


Figure 5-2. Effect of peptides on the aspect ratio (A), length (B), and the population (C) of COM crystals. Each measurement was performed with three separate batches. Error bar equals one standard deviation.

6. Interfacial Studies of Calcium Oxalate Monohydrate Crystal Growth

Atomic force microscopy (AFM) has proven to be a useful technique to analyze crystallization in a wide variety of systems, including biomaterials [85-87], polymers [88, 89], metals [90], and microporous materials [91, 92], such as in zeolites [53, 54]. For instance, calcite (the thermodynamically most stable polymorph of calcium carbonate) has been examined in the presence of modifiers such as poly(vinyl alcohols) [9], chiral amino acids [93], and magnesium [52]. Traditionally AFM has been used to characterize the topography of material surface; however, *in situ* AFM has made it possible to observe the events of nucleation and crystal growth in real time and at a microscopic level, which helps elucidate growth mechanisms for a variety of crystallization systems. Liquid sample cells permit precise control over the conditions of the experimental measurements, such as solution temperature, pH, ionic strength, composition, flow rate, etc.

As mentioned in Ch.1, citrate is a moderate inhibitor of COM crystal growth. There have been many studies reporting citrate's efficacy and also its interaction with COM crystal surfaces using AFM [52, 77, 93]. DeYoreo and coworkers in particular have been actively involved in AFM *in situ* analysis of COM crystal growth in the presence of citrate [52, 77, 93] and other biomolecules [24, 93, 94]. They observed the crystal growth behavior on both (-101) and (010) faces (note that crystal face indices used in these papers follow notation by Deganello [12] which are equivalent to the (100) and (010) faces, respectively, in this study) using different concentrations of citrate at supersaturation of 0.7 mM. COM crystals grow from dislocation sources

imbedded in crystal structure due to defects during synthesis. In the case of the (100) face, the growth hillocks are triangular shaped; and in the case of the (010) face, they exhibit rectangular shaped morphology. According to prior studies, citrate binds to (100) faces more strongly than to (010) faces [77]. *In situ* AFM studies revealed step pinning of the (100) face with the introduction of citrate at the concentration of 1.2×10^{-5} M [77]. Step pinning resulted in jagged steps and circular hillocks while images of the (010) face showed a slight rounding of edges. This study was also combined with molecular modeling to identify the potential binding mode of citrate on COM surfaces [77]. The following sections discuss the results of *in situ* AFM measurements that were used to examine crystal step growth and the effect of chondroitin sulfate, a urinary component and known inhibitor, on the growth of COM crystals.

6.1 Measurement of step advancement on the (010) surface

Step growth of COM crystals on the (010) surface was measured using two different methods. The first method was the ‘single-line scan’, which literally scans a single line along the x-direction and does not raster the AFM probe in the y-direction. AFM images were obtained by scanning the surface with a probe that tracks the height of features on the sample (see details of the procedure in Ch. 2). In brief, the AFM probe scans one line in x-direction and moves to the next line by repositioning in y-direction, which makes x-direction the fast axis and the y-direction the slow axis. Disabling the slow axis scan allows a single line scan to capture the dynamic changes in crystal surface topography (i.e., step advancement) more rapidly. A representative image is shown in Figure 6-1. The upper half part of Figure 6-1A (above the dashed white line) is a 2-D image of the growth hillock. The 2-D scan was switched to a line

scan near the center of the screw dislocation by disabling the slow axis scan (below the dashed white line in Figure 6-1A). As shown in Figure 6-1B, when the slow axis scan is disabled, the image is rendered a plot of time (y-axis) versus the line scan (x-axis). In order to measure the step growth velocity, an arbitrary reference line is drawn (this line should be distinctive and consistent throughout the set of images to be processed). The distance between each step within the hillock and the reference line was measured at different time points. The time of each scan was calculated by dividing the scan rate (Hz) by the number of lines per sample (an input parameter that was set to 256 lines/scan). This process was repeated for seven consecutive images (total imaging time equal to ca. 200 seconds).

The second method that was employed was a more traditional 2-D imaging in contact mode to capture the growth of steps on the (010) surface. The step velocity was obtained by measuring the distance between each step within the hillock and a preset reference line (i.e., some defect or surface feature that is consistent throughout the duration of AFM imaging). The AFM probe is rastered up and down the scanning area. For these analyses, the images selected were scanned in the same direction (i.e., scanning upward or scanning downward) to avoid any distortions due to the scan direction. As such, movies were generated with each frame taken every 63 seconds apart. This process was done with six images (total imaging time was ca. 315 seconds). Here we compare the $\langle 010 \rangle$ step velocities obtained from both methods. For the line scan images, the distances were measured from the right side of Figure 6-1B since the velocity measured from the left side was inconsistent, possibly due to impediment of step growth from smaller hillocks on its left (or possible impurities). The step growth velocity obtained from the first method was ca. 0.64 nm/s at

supersaturation of 3.7. For the second method, the step velocity was ca. 0.65 nm/s, which is in good agreement with the value obtained from the first method. These studies demonstrate that both methods are valid for measuring step growth velocity. There have been several reported values for the velocity in the literature; however, the conditions of each experiment vary in both composition of solutions (i.e., supersaturation) and the flow rate. A comparison of literature values with our work is provided in Table 6-1.

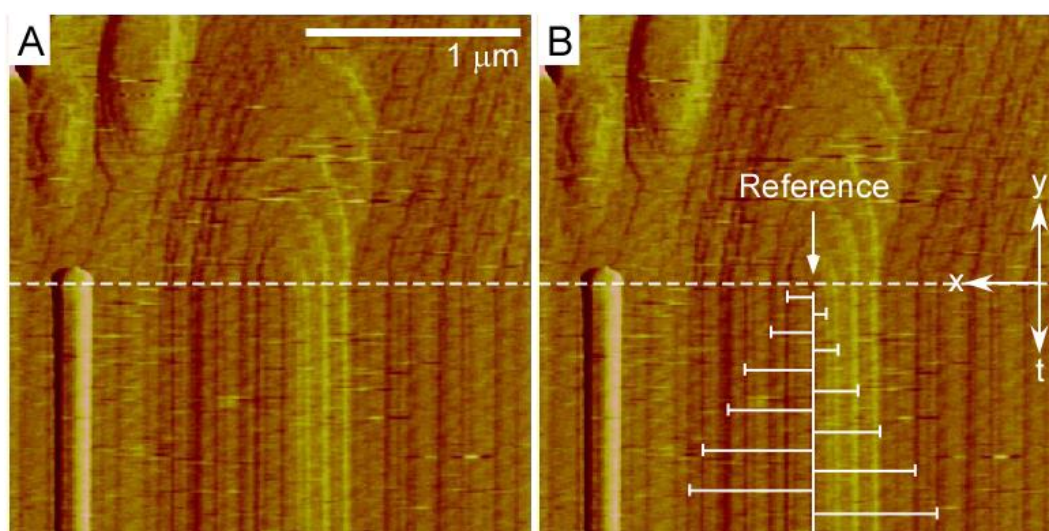


Figure 6-1. Demonstration of an AFM single-line scan method. The step velocity was obtained by measuring the distance between each step of the hillock and a reference line (labeled in B). The images shown here are in deflection mode.

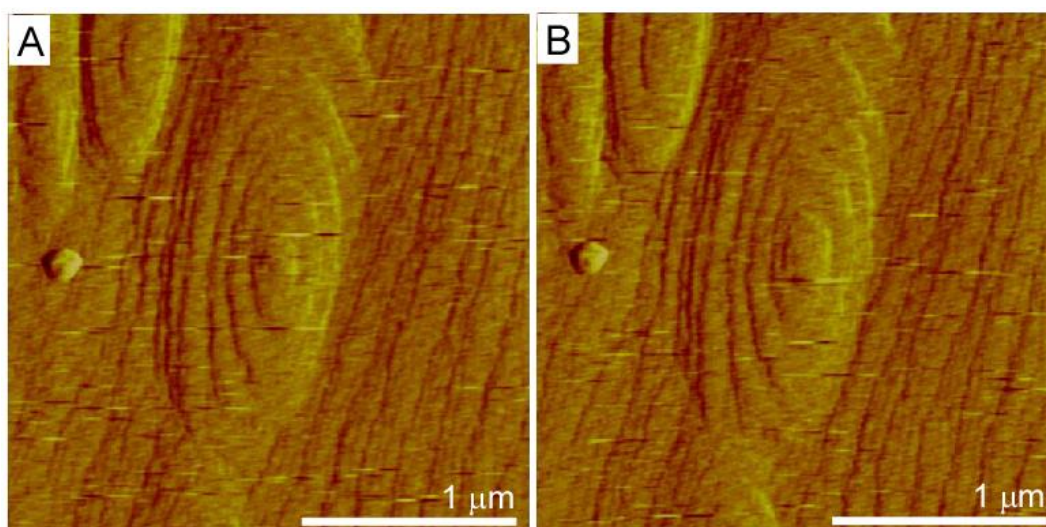


Figure 6-2. Consecutive deflection mode AFM images of growth hillocks growing in supersaturated calcium oxalate solution. The step velocity was obtained by measuring the change in step position with images taken in succession.

Table 6-1. Reported values of COM step velocity on the (010) surface.

| Group | Supersaturation | Velocity (nm/s) | | |
|-----------------|-----------------|-----------------|-------|--------|
| | | [001] | [100] | [12-1] |
| DeYoreo* [77] | 0.82 | 1.2 | | 0.8 |
| Rashkovich [56] | 4 - 7 | | 0.3 | |
| This work | 3.7 | | 0.65 | |

* The Miller indices originally defined by Deganello [12] were switched to our convention.

6.2 Effect of chondroitin sulfate on COM crystal growth

Here we used a model COM growth inhibitor, chondroitin sulfate, to benchmark *in situ* AFM studies of COM crystallization for future analysis of OGMs. Chondroitin sulfate A (C₄S) is a common urinary constituent that is believed to play

an inhibitory role in COM crystallization *in vivo*. This glycosaminoglycan contains a large percentage of negatively-charged groups, which is characteristic of effective COM growth inhibitors and suggests C₄S inhibits COM crystallization and potentially prevents COM crystal attachment to the negatively-charged epithelial cell surface of the kidney [88]. Moreover, the negatively charged carboxyl and/or sulfate groups of C₄S and its random coil structure add steric hinderance when C₄S is bound to COM crystals, which may also prevent crystal aggregation and attachment to epithelial cells [91]. Studies by Farmanesh et al. revealed that C₄S binds to the (010) surface of COM crystals rendering elongated crystals [95].

In this study, 1 and 5 µg/mL of C₄S was introduced in supersaturated calcium oxalate solution to examine the effect of inhibitor on growing hillocks in the (010) surface. Growth solutions ($s = 3.7$) in the absence of C₄S were first introduced to the COM crystals to quantify the step velocity of hillocks (control), as shown in Figure 6-3A and 3B. Growth hillocks on the (010) surface have diamond-shaped morphology bounded by {12-1} and {001} faces. Figure 6-3A and 3B clearly show that steps on the hillocks are advancing with time (image 3B was taken 10 minutes after 3A). Also, a distinct dislocation source and the spiral growth pattern were observed in Figure 3B. Two-dimensional island formation on step edges and an increase in the height of step edges were triggered by the introduction of 1 µg/mL of C₄S, as shown in Figure 6-3C and 3D, respectively. The step height of hillocks for the control surface was ca. 1 – 2 nm, which is on the order of one unit cell in the b-axis (14.58 Å); however, the step height increased up to 3 nm in the presence of 1 µg/mL of C₄S, which suggests that C₄S binds to {12-1} steps and slows the rate of layer advancement across the (010) surface. In the presence of 5 µg/mL C₄S, COM hillock growth was completely

suppressed after one minute of imaging, as shown in Figure 6-3F and 3G where latter was imaged after one minute. Growth inhibition results in a roughening of the surface and the disappearance of well-defined steps. Interestingly, hillock growth can be regenerated by replacing the C_4S -containing solution with supersaturated calcium oxalate solution (in the absence of inhibitor). As shown in Figure 6-3H, the hillocks did return to their original state, which indicates that C_4S was not incorporated into the growing crystal surface, but rather was merely physisorbed to the surfaces and could readily be desorbed with the replenishment of growth solution. Similar regeneration behavior was reported for the resurrection of potassium dihydrogen phosphate from dead zone by DeYoreo [77] and polyamino acids by Ward.

In attempt to optimize the observation of crystal growth at a molecular level, we have tested various solution conditions i.e., different supersaturation, and we were able to quantify the hillock step growth of COM crystals on (010) face. Also we have successfully observed the effect of a growth modifier on the growth of COM crystal in real time at a microscopic level. These establishments will serve as a platform in future work where the effect of other growth modifiers e.g., OGMs and peptides will be systematically examined.

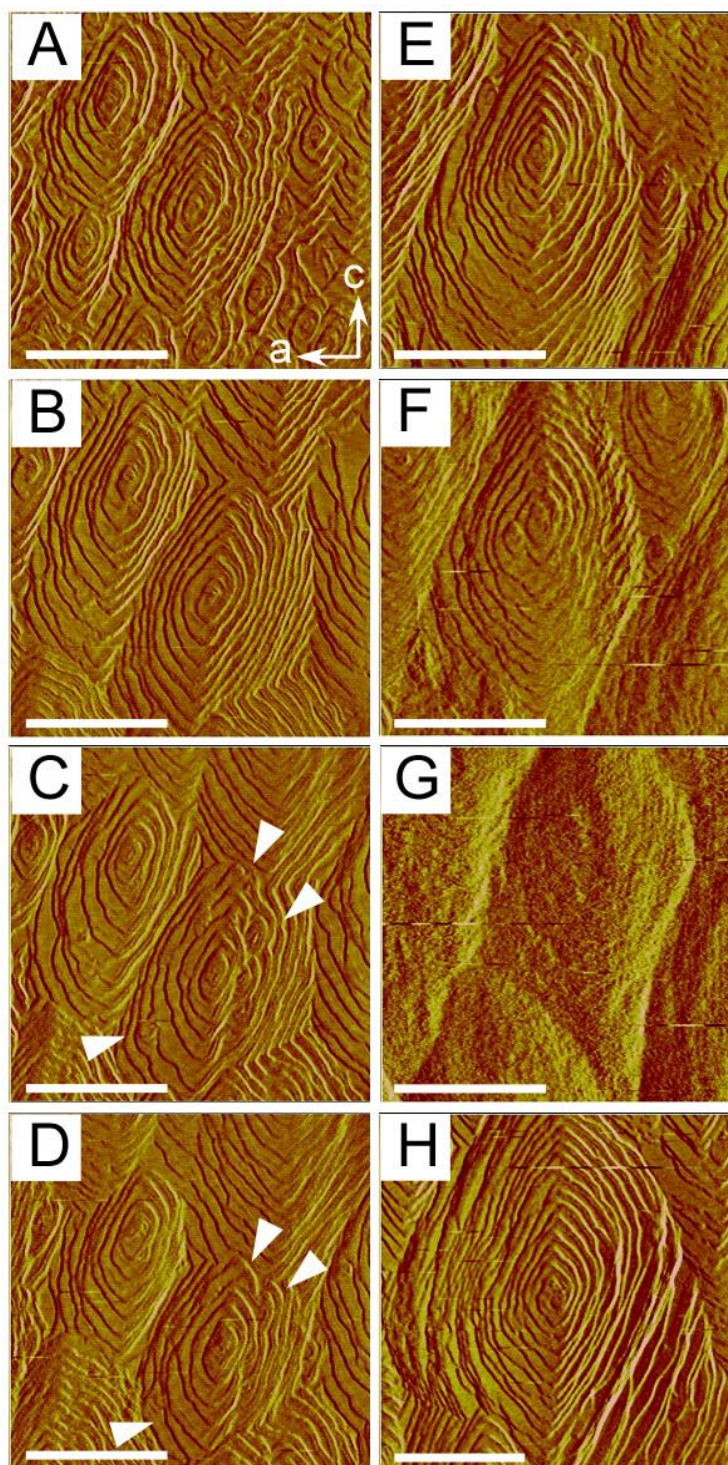


Figure 6-3. *In situ* AFM images of growth hillocks on a (010) surface. Time-elapsd images were taken at an initial time (A) and after 10 minutes of growth (B). Images C – E show the effect of 1 $\mu\text{g/mL}$ -C₄S on hillock growth. These studies reveal the formation of 2-D islands (C) and an increase in the height of steps (D), as indicated by the arrows. Images F and G show the effect of 5 $\mu\text{g/mL}$ C₄S on hillock growth. After one minute growth is complete arrested (G). Image H shows the recovery of growth hillocks upon removal of C₄S from the growth solution. Scale bars indicate 1 μm .

7. Conclusion

Inhibition of calcium oxalate monohydrate crystallization was examined using small organic molecules, a tailored peptide library and a native glycosaminoglycan in urine (chondroitin sulfate A). The selection of these growth modifiers were inspired from past studies. A preliminary study by Asplin et al. where the efficacy of citrate, a moderate inhibitor of COM crystals, was compared to that of hydroxycitrate, a structural analogue to citrate with one additional hydroxyl group, triggered an interesting idea to compare the effects of other citrate analogues on COM crystallization. In addition, the design of *de novo* peptide sequences and the judicious selection of a binder and a spacer were guided by studies of calcium-binding proteins, which inhibit or modify the kinetics of calcification, possess a large fraction of L-aspartic acid groups. To this end, we have attempted to investigate the physicochemical role of functional groups in growth modifiers. It was found that the number of hydroxyl groups and carboxyl groups do play an important role in both the efficacy and specificity of the growth modifiers. A comparison of OGMs at the same concentration (60 µg/mL) revealed that increasing the number of carboxyl groups resulted in a slight decrease in the aspect ratio of COM crystals and a sharp increase in percent inhibition. Also, increasing the number of hydroxyl groups tends to improve the efficacy of modifiers; however, it may also impose steric hindrance to binding of modifiers to COM crystal surfaces.

A comparison of COM crystals prepared with different peptides revealed two types of morphologies: Hexagonal platelets and diamond-shaped crystals. The percentage of diamond platelets was indicative of a peptide's effectiveness to reduce COM growth along the primary [12-1] growth direction. Interestingly, OGMs and

peptides reduced the [001]/[010] aspect ratio of COM crystals, which indicated their preferential binding to {12-1} surfaces. As previously mentioned, different crystallographic planes of COM crystals have different orientations of oxalate molecules. The orientation of carboxyl groups in the modifiers selected in this study ostensibly exhibit preferable interactions with the {12-1} surfaces.

In situ AFM was employed to examine the kinetics of COM crystal step growth and the interfacial interaction of a known inhibitor, C₄S, with the COM (010) surface. It was observed that in the presence of C₄S, steps of growth hillocks were pinned resulting in jagged step edges and the complete arrested growth at elevated inhibitor concentration. Also, the recovery of hillocks with the removal of C₄S after complete arrest of growth was observed. The results from this *in situ* AFM study will serve as a benchmark for future initiatives aimed to more systematically quantify modifier-crystal interfacial interactions.

The results obtained in this study identify promising inhibitors of COM crystallization towards the discovery of more effective preventative treatments of kidney stone disease. Current treatment therapy involves increased water intake and diet regulation, which collectively decrease the supersaturation of calcium oxalate in urine; however, these treatments do not suppress the formation of COM stones. We believe that results obtained in this work and further studies to optimize COM growth inhibition may prove useful in developing novel drugs for nephrolithiasis.

References

1. Coe, F.L. and Asplin, J.R., *Stopping the stones*. Science, 2010. **330**(6002): p. 325-326.
2. Dyer, R. and Nordin, B.E.C., *Urinary crystals and their relation to stone formation*. Nature, 1967. **215**(5102): p. 751.
3. Elliot, J.S. and Rabinowitz, I.N., *Calcium-oxalate crystalluria - Crystal size in urine*. Journal of Urology, 1980. **123**(3): p. 324-327.
4. Sheng, X.X., Jung, T.S., Wesson, J.A., and Ward, M.D., *Adhesion at calcium oxalate crystal surfaces and the effect of urinary constituents*. Proceedings of the National Academy of Sciences of the United States of America, 2005. **102**(2): p. 267-272.
5. Coe, F.L., Parks, J.H., and Asplin, J.R., *Medical progress - The pathogenesis and threatment of kidney stones*. New England Journal of Medicine, 1992. **327**(16): p. 1141-1152.
6. Scheinman, S.J., Cox, J.P.D., Lloyd, S.E., Pearce, S.H.S., Salenger, P.V., Hoopes, R.R., Bushinsky, D.A., Wrong, O., Asplin, J.R., Langman, C.B., Norden, A.G.W., and Thakker, R.V., *Isolated hypercalciuria with mutation in CLCN5: Relevance to idiopathic hypercalciuria*. Kidney International, 2000. **57**(1): p. 232-239.
7. Bushinsky, D.A., *Nephrolithiasis*. Journal of the American Society of Nephrology, 1998. **9**(5): p. 917-924.
8. Asplin, J.R., *Hyperoxaluric calcium nephrolithiasis*. Endocrinology and Metabolism Clinics of North America, 2002. **31**(4): p. 927.

9. Pak, C.Y.C., *Citrate and renal calculi- An update*. Mineral and Electrolyte Metabolism, 1994. **20**(6): p. 371-377.
10. Pak, C.Y.C., Sakhaee, K., Crowther, C., and Brinkley, L., *Evidence justifying a high fluid intake in treatment of nephrolithiasis*. Annals of Internal Medicine, 1980. **93**(1): p. 36-39.
11. Borghi, L., Meschi, T., Amato, F., Briganti, A., Novarini, A., and Giannini, A., *Urinary volume, water and recurrences in idiopathic calcium nephrolithiasis: A 5-year randomized prospective study*. Journal of Urology, 1996. **155**(3): p. 839-843.
12. Loe, Y.C.C., Bergeron, N., Rodriguez, N., and Schwarz, J.M., *Gas chromatography/mass spectrometry method to quantify blood hydroxycitrate concentration*. Analytical Biochemistry, 2001. **292**(1): p. 148-154.
13. Tazzoli, V. and Domeneghetti, C., *The crystal-structures of whewellite and weddellite - reexamination and comparison*. American Mineralogist, 1980. **65**(3-4): p. 327-334.
14. Gilmer, G.H., Ghez, R., and Cabrera, N., *Analysis of combined surface and volume diffusion processes in crystal growth*. Journal of Crystal Growth, 1971. **8**(1): p. 79.
15. Brown, H.C., Braude, E.A., and Nachod, F.C., *Determination of organic structures by physical methods*. Vol. 5. 1955, New York: Academic Press.
16. Gasperino, D., Yeckel, A., Olmsted, B.K., Ward, M.D., and Derby, J.J., *Mass transfer limitations at crystallizing interfaces in an atomic force microscopy fluid cell: A finite element analysis*. Langmuir, 2006. **22**(15): p. 6578-6586.

17. Weissbuch, I., Addadi, L., Lahav, M., and Leiserowitz, L., *Molecular recognition at crystal interfaces*. Science, 1991. **253**(5020): p. 637-645.
18. Weissbuch, I., Lahav, M., and Leiserowitz, L., *Toward stereochemical control, monitoring, and understanding of crystal nucleation*. Crystal Growth & Design, 2003. **3**(2): p. 125-150.
19. Lahav, M. and Leiserowitz, L., *A stereochemical approach that demonstrates the effect of solvent on the growth of polar crystals: A perspective*. Crystal Growth & Design, 2006. **6**(3): p. 619-624.
20. Sizemore, J.P. and Doherty, M.F., *A new model for the effect of molecular imposters on the shape of faceted molecular crystals*. Crystal Growth & Design, 2009. **9**(6): p. 2637-2645.
21. Antinozzi, P.A., Brown, C.M., and Purich, D.L., *Calcium oxalate monohydrate crystallization- Citrate inhibition of nucleation and growth steps*. Journal of Crystal Growth, 1992. **125**(1-2): p. 215-222.
22. Millan, A., Sohnle, O., and Grases, F., *The influence of crystal morphology on the kinetics of growth of calcium oxalate monohydrate*. Journal of Crystal Growth, 1997. **179**(1-2): p. 231-239.
23. Sayan, P., Sargut, S.T., and Kiran, B., *Calcium oxalate crystallization in the presence of amino acids, proteins and carboxylic acids*. Crystal Research and Technology, 2009. **44**(8): p. 807-817.
24. Wang, L.J., Qiu, S.R., Zachowicz, W., Guan, X.Y., DeYoreo, J.J., Nancollas, G.H., and Hoyer, J.R., *Modulation of calcium oxalate crystallization by linear aspartic acid-rich peptides*. Langmuir, 2006. **22**(17): p. 7279-7285.

25. Asplin, J., Deganello, S., Nakagawa, Y.N., and Coe, F.L., *Evidence that nephrocalcin and urine inhibit nucleation of calcium oxalate monohydrate crystals*. American Journal of Physiology, 1991. **261**(5): p. F824-F830.
26. Grases, F., Gil, J.J., and Conte, A., *Glycosaminoglycans: Inhibition of calcium oxalate crystalline growth and promotion of crystal aggregation*. Colloids and Surfaces, 1989. **36**(1): p. 29-38.
27. Angell, A.H. and Resnick, M.I., *Surface interaction between glycosaminoglycans and calcium oxalate*. Journal of Urology, 1989. **141**(5): p. 1255-1258.
28. Robertso.Wg, Peacock, M., and Nordin, B.E.C., *Inhibitors of growth and aggregation of calcium oxalate crystals in vitro*. Clinica Chimica Acta, 1973. **43**(1): p. 31-37.
29. Fellstrom, B., Danielson, B.G., Ljunghall, S., and Wikstrom, B., *Crystal inhibition - The effects of polyanions on calcium oxalate crystal growth*. Clinica Chimica Acta, 1986. **158**(3): p. 229-235.
30. Grohe, B., O'Young, J., Ionescu, D.A., Lajoie, G., Rogers, K.A., Karttunen, M., Goldberg, H.A., and Hunter, G.K., *Control of calcium oxalate crystal growth by face-specific adsorption of an osteopontin phosphopeptide*. Journal of the American Chemical Society, 2007. **129**(48): p. 14946-14951.
31. Hug, S., Grohe, B., Jalkanen, J., Chan, B., Galarreta, B., Vincent, K., Lagugne-Labarthe, F., Lajoie, G., Goldberg, H.A., Karttunen, M., and Hunter, G.K., *Mechanism of inhibition of calcium oxalate crystal growth by an osteopontin phosphopeptide*. Soft Matter, 2012. **8**(4): p. 1226-1233.

32. Langdon, A., Wignall, G.R., Rogers, K., Sorensen, E.S., Denstedt, J., Grohe, B., Goldberg, H.A., and Hunter, G.K., *Kinetics of Calcium Oxalate Crystal Growth in the Presence of Osteopontin Isoforms: An Analysis by Scanning Confocal Interference Microscopy*. *Calcified Tissue International*, 2009. **84**(3): p. 240-248.
33. Taller, A., Grohe, B., Rogers, K.A., Goldberg, H.A., and Hunter, G.K., *Specific adsorption of osteopontin and synthetic polypeptides to calcium oxalate monohydrate crystals*. *Biophysical Journal*, 2007. **93**(5): p. 1768-1777.
34. Hess, B., *The role of Tamm-Horsfall glycoprotein and nephrocalcin in calcium oxalate monohydrate crystallization processes*. *Scanning Microscopy*, 1991. **5**(3): p. 689-696.
35. Gul, A. and Rez, P., *Models for protein binding to calcium oxalate surfaces*. *Urological Research*, 2007. **35**(2): p. 63-71.
36. Edyvane, K.A., Ryall, R.L., Mazzachi, R.D., and Marshall, V.R., *The effect of serum on the crystallization of calcium oxalate in whole human urine: Inhibition disguised as apparent promotion*. *Urological Research*, 1987. **15**(2): p. 87-92.
37. Ryall, R.L., Harnett, R.M., Hibberd, C.M., Edyvane, K.A., and Marshall, V.R., *Effects of chondroitin sulfate, human serum albumin and Tamm-Horsfall mucoprotein on calcium oxalate crystallization in undiluted human urine*. *Urological Research*, 1991. **19**(3): p. 181-188.
38. Wesson, J.A., Ganne, V., Beshensky, A.M., and Kleinman, J.G., *Regulation by macromolecules of calcium oxalate crystal aggregation in stone formers*. *Urological Research*, 2005. **33**(3): p. 206-212.

39. Fleming, D.E., van Bronswijk, W., and Ryall, R.L., *A comparative study of the adsorption of amino acids on to calcium minerals found in renal calculi*. Clinical Science, 2001. **101**(2): p. 159-168.
40. Wesson, J.A., Johnson, R.J., Mazzali, M., Beshensky, A.M., Stietz, S., Giachelli, C., Liaw, L., Alpers, C.E., Couser, W.G., Kleinman, J.G., and Hughes, J., *Osteopontin is a critical inhibitor of calcium oxalate crystal formation and retention in renal tubules*. Journal of the American Society of Nephrology, 2003. **14**(1): p. 139-147.
41. Mo, L., Liaw, L., Evan, A.P., Sommer, A.J., Lieske, J.C., and Wu, X.R., *Renal calcinosis and stone formation in mice lacking osteopontin, Tamm-Horsfall protein, or both*. American Journal of Physiology-Renal Physiology, 2007. **293**(6): p. F1935-F1943.
42. Grohe, B., Chan, B.P.H., Sorensen, E.S., Lajoie, G., Goldberg, H.A., and Hunter, G.K., *Cooperation of phosphates and carboxylates controls calcium oxalate crystallization in ultrafiltered urine*. Urological Research, 2011. **39**(5): p. 327-338.
43. Wang, L.J., Guan, X.Y., Tang, R.K., Hoyer, J.R., Wierzbicki, A., De Yoreo, J.J., and Nancollas, G.H., *Phosphorylation of osteopontin is required for inhibition of calcium oxalate crystallization*. Journal of Physical Chemistry B, 2008. **112**(30): p. 9151-9157.
44. Hess, B., Nakagawa, Y., Parks, J.H., and Coe, F.L., *Molecular abnormality of Tamm-Horsfall glycoprotein in calcium oxalate nephrolithiasis*. American Journal of Physiology, 1991. **260**(4): p. F569-F578.

45. Ronco, P., Brunisholz, M., Geniteau-Legendre, M., Chatelet, F., Verroust, P., and Richet, G., *Physiopathologic aspects of Tamm-Horsfall protein: a phylogenetically conserved marker of the thick ascending limb of Henle's loop*. Advances in nephrology from the Necker Hospital, 1987. **16**: p. 231-49.
46. Scurr, D.S. and Robertson, W.G., *Modifiers of calcium oxalate crystallization found in urine. 3. Studies on the role of Tamm-Horsfall mucoprotein and of ionic strength*. Journal of Urology, 1986. **136**(2): p. 505-507.
47. Boyce, W.H. and King, J.S., *I. Some special aspects of metabolic dysfunction- Present concepts concerning origin of matrix and stones*. Annals of the New York Academy of Sciences, 1963. **104**(2): p. 563.
48. Hallson, P.C. and Rose, G.A., *Uromucoids and urinary stone formation*. Lancet, 1979. **1**(8124): p. 1000-1002.
49. Viswanathan, P., Rimer, J.D., Kolbach, A.M., Ward, M.D., Kleinman, J.G., and Wesson, J.A., *Calcium oxalate monohydrate aggregation induced by aggregation of desialylated Tamm-Horsfall protein*. Urological Research, 2011. **39**(4): p. 269-282.
50. Knorle, R., Schnierle, P., Koch, A., Buchholz, N.P., Hering, F., Seiler, H., Ackermann, T., and Rutishauser, G., *Tamm-Horsfall glycoprotein- Role in inhibition and promotion of renal calcium oxalate stone formation studied with Fourier-transform infrared spectroscopy*. Clinical Chemistry, 1994. **40**(9): p. 1739-1743.
51. Pragasam, V., Kalaiselvi, P., Subashini, B., Sumitra, K., and Varalakshmi, P., *Structural and functional modification of THP on nitration: comparison with stone formers THP*. Nephron. Physiology, 2005. **99**(1): p. p28-34.

52. Stephenson, A.E., Hunter, J.L., Han, N., DeYoreo, J.J., and Dove, P.M., *Effect of ionic strength on the Mg content of calcite: Toward a physical basis for minor element uptake during step growth*. *Geochimica Et Cosmochimica Acta*, 2011. **75**(15): p. 4340-4350.
53. Lupulescu, A.I., Kumar, M., and Rimer, J.D., *A facile strategy to design zeolite L crystals with tunable morphology and surface architecture*. *Journal of the American Chemical Society*, 2013.
54. Lupulescu, A.I. and Rimer, J.D., *Tailoring silicalite-1 crystal morphology with molecular modifiers*. *Angewandte Chemie-International Edition*, 2012. **51**(14): p. 3345-3349.
55. Guo, S.W., Ward, M.D., and Wesson, J.A., *Direct visualization of calcium oxalate monohydrate crystallization and dissolution with atomic force microscopy and the role of polymeric additives*. *Langmuir*, 2002. **18**(11): p. 4284-4291.
56. Gvozdev, N.V., Petrova, E.V., Chernevich, T.G., Shustin, O.A., and Rashkovich, L.N., *Atomic force microscopy of growth and dissolution of calcium oxalate monohydrate (COM) crystals*. *Journal of Crystal Growth*, 2004. **261**(4): p. 539-548.
57. Petrova, E.V., Gvozdev, N.V., and Rashkovich, L.N., *Growth and dissolution of calcium oxalate monohydrate (COM) crystals*. *Journal of Optoelectronics and Advanced Materials*, 2004. **6**(1): p. 261-268.
58. Ryall, R.L., Harnett, R.M., and Marshall, V.R., *The effect of urine, pyrophosphate, citrate, magnesium and glycosaminoglycans on the growth*

- and aggregation of calcium-oxalate crystals invitro. Clinica Chimica Acta*, 1981. **112**(3): p. 349-356.
59. Dawson, R.M.C., Elliott, D.C., Elliott, W.H., and Jones, K.M., *Data for biochemical reserach*. 3 ed1989, USA: Oxford University Press 592.
 60. Chernov, A.A., Petrova, E., and Rashkovich, L.N., *Dependence of the CaOx and MgOx growth rate on solution stoichiometry. Non-Kossel crystal growth. Journal of Crystal Growth*, 2006. **289**(1): p. 245-254.
 61. Grohe, B., Hug, S., Langdon, A., Jalkanen, J., Rogers, K.A., Goldberg, H.A., Karttunen, M., and Hunter, G.K., *Mimicking the biomolecular control of calcium oxalate monohydrate crystal growth: Effect of contiguous glutamic acids. Langmuir*, 2012. **28**(33): p. 12182-12190.
 62. Thongboonkerd, V., Semangoen, T., and Chutipongtanate, S., *Factors determining types and morphologies of calcium oxalate crystals: Molar concentrations, buffering, pH, stirring and temperature. Clinica Chimica Acta*, 2006. **367**(1-2): p. 120-131.
 63. Borden, T.A. and Lyon, E.S., *Effects of magnesium and pH on experimental calcium oxalate stone disease. Investigative Urology*, 1969. **6**(4): p. 412.
 64. Verplaetse, H., Verbeeck, R.M.H., Verbaeys, A., and Oosterlinck, W., *Solubility of calcium-oxalate monohydrate and hydroxyapatite in EDTA solutions. Journal of Urology*, 1986. **135**(3): p. 608-611.
 65. Desmars, J.F. and Tawashi, R., *Dissolution and growth of calcium oxalate monohydrate. 1. Effect of magnesium and pH. Biochimica Et Biophysica Acta*, 1973. **313**(2): p. 256-267.

66. Verplaetse, H., Verbeeck, R.M.H., Minnaert, H., and Oosterlinck, W., *Solubility of inorganic kidney-stone components in the presence of acid-base sensitive complexing agents*. European Urology, 1985. **11**(1): p. 44-51.
67. Ulmgren, P. and Radestrom, R., *An equilibrium model of the solubility of calcium oxalate in sodium chloride medium*. Nordic Pulp & Paper Research Journal, 1999. **14**(3): p. 214-220.
68. Streit, J., Tran-Ho, L.C., and Konigsberger, E., *Solubility of the three calcium oxalate hydrates in sodium chloride solutions and urine-like liquors*. Monatshefte Fur Chemie, 1998. **129**(12): p. 1225-1236.
69. Burns, J.R. and Finlayson, B., *A proposal for a standard reference artificial urine in in vitro urolithiasis experiments*. Investigative Urology, 1980. **18**(2): p. 167-169.
70. Kim, I.W., DiMasi, E., and Evans, J.S., *Identification of mineral modulation sequences within the nacre-associated oyster shell protein, n16*. Crystal Growth & Design, 2004. **4**(6): p. 1113-1118.
71. Dalas, E., Chalias, A., Gatos, D., and Barlos, K., *The inhibition of calcium carbonate crystal growth by the cysteine-rich Mdm2 peptide*. Journal of Colloid and Interface Science, 2006. **300**(2): p. 536-542.
72. Parks, J.H., Coward, M., and Coe, F.L., *Correspondence between stone composition and urine supersaturation in nephrolithiasis*. Kidney International, 1997. **51**(3): p. 894-900.
73. Michenfelder, M., Fu, G., Lawrence, C., Weaver, J.C., Wustman, B.A., Taranto, L., Evans, J.S., and Morsel, D.E., *Characterization of two molluscan*

- crystal-modulating biomineralization proteins and identification of putative mineral binding domains*. Biopolymers, 2003. **70**(4): p. 522-533.
74. Kim, I.W., Morse, D.E., and Evans, J.S., *Molecular characterization of the 30-AA N-terminal mineral interaction domain of the biomineralization protein AP7*. Langmuir, 2004. **20**(26): p. 11664-11673.
 75. Sugawara, A., Nishimura, T., Yamamoto, Y., Inoue, H., Nagasawa, H., and Kato, T., *Self-organization of oriented calcium carbonate/polymer composites: Effects of a matrix peptide isolated from the exoskeleton of a crayfish*. Angewandte Chemie-International Edition, 2006. **45**(18): p. 2876-2879.
 76. Grohe, B., O'Young, J., Langdon, A., Karttunen, M., Goldberg, H.A., and Hunter, G.K., *Citrate Modulates Calcium Oxalate Crystal Growth by Face-Specific Interactions*. Cells Tissues Organs, 2011. **194**(2-4): p. 176-181.
 77. Land, T.A., Martin, T.L., Potapenko, S., Palmore, G.T., and De Yoreo, J.J., *Recovery of surfaces from impurity poisoning during crystal growth*. Nature, 1999. **399**(6735): p. 442-445.
 78. Jung, T., Sheng, X.X., Choi, C.K., Kim, W.S., Wesson, J.A., and Ward, M.D., *Probing crystallization of calcium oxalate monohydrate and the role of macromolecule additives with in situ atomic force microscopy*. Langmuir, 2004. **20**(20): p. 8587-8596.
 79. Qiu, S.R., Wierzbicki, A., Orme, C.A., Cody, A.M., Hoyer, J.R., Nancollas, G.H., Zepeda, S., and De Yoreo, J.J., *Molecular modulation of calcium oxalate crystallization by osteopontin and citrate*. Proceedings of the National Academy of Sciences of the United States of America, 2004. **101**(7): p. 1811-1815.

80. Wang, L.J., Zhang, W., Qiu, S.R., Zachowicz, W.J., Guan, X.Y., Tang, R.K., Hoyer, J.R., De Yoreo, J.J., and Nancollas, G.H., *Inhibition of calcium oxalate monohydrate crystallization by the combination of citrate and osteopontin*. Journal of Crystal Growth, 2006. **291**(1): p. 160-165.
81. Graether, S.P., Kuiper, M.J., Gagne, S.M., Walker, V.K., Jia, Z.C., Sykes, B.D., and Davies, P.L., *beta-helix structure and ice-binding properties of a hyperactive antifreeze protein from an insect*. Nature, 2000. **406**(6793): p. 325-328.
82. Marshall, C.B., Fletcher, G.L., and Davies, P.L., *Hyperactive antifreeze protein in a fish*. Nature, 2004. **429**(6988): p. 153-153.
83. Doxey, A.C., Yaish, M.W., Griffith, M., and McConkey, B.J., *Ordered surface carbons distinguish antifreeze proteins and their ice-binding regions*. Nature Biotechnology, 2006. **24**(7): p. 852-855.
84. Farmanesh, S., Chung, J., Chandra, D., Sosa, R.D., Karande, P., and Rimer, J.D., *High-throughput platform for design and screening of peptides as inhibitors of calcium oxalate monohydrate crystallization*. Journal of Crystal Growth, 2013.
85. Kok, D.J. and Khan, S.R., *Calcium-oxalate nephrolithiasis, a free or fixed particle disease*. Kidney International, 1994. **46**(3): p. 847-854.
86. Shiraga, H., Min, W., Vandusen, W.J., Clayman, M.D., Miner, D., Terrell, C.H., Sherbotie, J.R., Foreman, J.W., Przysiecki, C., Neilson, E.G., and Hoyer, J.R., *Inhibition of calcium-oxalate crystal growth in vitro by uropontin: Another member of the aspartic acid-rich protein superfamily*. Proceedings of

- the National Academy of Sciences of the United States of America, 1992. **89**(1): p. 426-430.
87. Tiselius, H.G., *Aspects on estimation of the risk of calcium-oxalate crystallization in urine*. Urologia Internationalis, 1991. **47**(4): p. 255-259.
 88. Lieske, J.C., Leonard, R., and Toback, F.G., *Adhesion of calcium-oxalate monohydrate crystals to renal epithelial cells is inhibited by specific anions*. American Journal of Physiology-Renal Fluid and Electrolyte Physiology, 1995. **268**(4): p. F604-F612.
 89. Borges, F.T., Michelacci, Y.M., Aguiar, J.A.K., Dalboni, M.A., Garofalo, A.S., and Schor, N., *Characterization of glycosaminoglycans in tubular epithelial cells: Calcium oxalate and oxalate ions effects*. Kidney International, 2005. **68**(4): p. 1630-1642.
 90. Gjaldbaek, J.C., *Inhibition of chondroitin sulfate and heparin on the growth and agglomeration of calcium-oxalate monohydrate crystals in vitro*. Clinica Chimica Acta, 1982. **120**(3): p. 363-365.
 91. Marszalek, P.E., Oberhauser, A.F., Li, H.B., and Fernandez, J.M., *The force-driven conformations of heparin studied with single molecule force microscopy*. Biophysical Journal, 2003. **85**(4): p. 2696-2704.
 92. Govindaraj, A. and Selvam, R., *Increased calcium oxalate crystal nucleation and aggregation by peroxidized protein of human kidney stone matrix and renal cells*. Urological Research, 2001. **29**(3): p. 194-198.
 93. Orme, C.A., Noy, A., Wierzbicki, A., McBride, M.T., Grantham, M., Teng, H.H., Dove, P.M., and DeYoreo, J.J., *Formation of chiral morphologies*

- through selective binding of amino acids to calcite surface steps.* Nature, 2001. **411**(6839): p. 775-779.
94. Weaver, M.L., Qiu, S.R., Hoyer, J.R., Casey, W.H., Nancollas, G.H., and De Yoreo, J.J., *Surface Aggregation of Urinary Proteins and Aspartic Acid-Rich Peptides on the Faces of Calcium Oxalate Monohydrate Investigated by In Situ Force Microscopy.* Calcified Tissue International, 2009. **84**(6): p. 462-473.
95. Farmanesh, S., Ramamoorthy, S., Asplin, J.R., Karande, P., and Rimer, J.D., *Inhibition of calcium oxalate monohydrate crystallization by urinary constituents in kidney stone matrix.* in preparation.